Università degli Studi di Padova

DIPARTIMENTO DI FISICA E ASTRONOMIA "GALILEO GALILEI"
Corso di Laurea Magistrale in Fisica

Tesi di laurea magistrale

Fabrication and characterization of nanostructured silicon microparticles with elevated drugloading capacity

Laureando:
Anna Lion
Matricola 1040049

Relatore:
Prof. Cinzia Sada

Relatore esterno:
Prof. Marina Scarpa
Universitá degli Studi di Trento

Anno Accademico 2014-2015

Contents

Acknowledgement

I want to thank all the people that helped me to get to this point. In particular I want to thank Prof. Cinzia Sada for believing in me and providing me the opportunity to work on this project. My supervisor Prof. Marina Scarpa for having introduced me to the lab world of nanomaterials, for all her help and constant availability. Dr. Paolo Bettotti for the advices, for teaching me about porous silicon preparation and for helping me with the experimental setup. My labmates, Cecilia, Sanjay, Elena and Chiara to have lightened my days in the lab and for all the fruitful discussions. My friends: Allegra, Franci, for providing me a sweet home when I was homeless (thanks also to Matteo and Giulia!!) and for putting up with me during these last few crazy weeks. My roomates and in particular Sara for sharing with me so many good (and bad) moments and for tooking care of me when I was in need. Daniele for always putting a smile on my face with all our crazy conversation. Marco and Elisa for sticking with me despite the distances and the difficulties, you are the best. Stefano for the good times and for alway believing in me. My whole family, for the unconditional love, the fight, the food, for being always there for me and for everything else. In particular my brother Luca, is it really necessary to say why?!(the pancakes at 4:30 were the best..almost!)

A thanks also to Dr. Nadhira Bensaada Laidani (Bruno Kessler Foundation-Trento) for the XPS measurements and data analysis.

A particular thanks to Ali Ghafarinazari, Emanuele Zera, Marina Scarpa, Gian Domenico Sorarú, Gino Mariotto, Nicola Daldosso for the work done togheter for "Isoconversional Kinetics of Thermal Oxidation of Mesoporous Silicon".

Materials and instrumentation

In this section we present an overview of instrumentation and materials used during this work for preparation, modification and characterization of nanostructured sample. Methods will be described when necessary in the next sections.

Chemicals
All chemicals were used as received without further purification.

- 1-Heptene, purum ≥99%, $CH_3(CH_2)_4CH = CH_2$, Sigma-Aldrich.
- Pentane, $CH_3(CH_2)_3CH_3$, Sigma-Aldrich.
- Toluene, $C_6H_5CH_3$, Sigma-Aldrich.
- 11-Bromo-1-undecene, purum ≥95.0% (GC), $Br(CH_2)_9CHCH_2$, Sigma-Aldrich.
- Acrylic acid, $CH_2 = CHCOOH$, purum ≥99%, Sigma-Aldrich.

Voltage/Current Generator
The current generators used to electrochemically etch silicon wafers were:

- Keithlet 2400, sourcemeter
- TTi CPX 400DP Dual 420 Watt, DC Power supply, Powerflex.

Agitator/Hot Plate
Agitator used during the functionalization procedure was: ARBO power.

Centrifuge
the centrifuges used during the functionalization procedure were:

- Universal 320, Hettich Zentrifugen
- MIKRO 120, Hettich Zentrifugen.

Weight measurements
Gravinometrical measurements were performed on a Sartorius precision balance (precision $10\mu g$).

Sonication
P-Si samples were sonicated in a UNISET AC2 Emmegi ultrasonic bath, with power set to 200Watt.

Spectrophotometer
Luminescence was measured with a Varian Cary Eclipse Fluorescence Spectrometer.

FTIR
Luminescence was measured with a micro-FTIR Nicolet iN10.

XPS
Luminescence was measured with a Scienta ESCA 200 at FBK(Bruno Kessler Foundation).

RAMAN
Luminescence was measured with a HORIBA Scientific LabRAM ARAMIS.

Optical images
All optical images were acquired using XploRA ONE microscope.

Introduction

Nanoscience aim is the study of the special properties that materials can acquire when their dimensions are reduced below 100nm and to understand how to exploit them for the creation of new material whose application range from electronics to biomedicine. Nanoparticles are of great scientific interest as they are effectively a bridge between bulk materials and atomic or molecular structures. A bulk material should have constant physical properties regardless of its size, but at the nano-scale this is often not the case. Size-dependent properties are observed such as quantum confinement in semiconductor particles, surface plasmon resonance in some metal particles and superparamagnetism in magnetic materials.
[7] Nanoparticles or nanocrystals made of metals, semiconductors, or oxides are of particular interest for their mechanical, electrical, magnetic, optical, chemical and other properties. Nanoparticles have been used as quantum dots and as chemical catalysts such as nanomaterial-based catalysts. Recently, a range of nanoparticles are extensively investigated for biomedical applications including tissue engineering, drug delivery, biosensor.[1]
A peculiar class of nanomaterial are those obtained from semiconductors. Due to their ability to emit light, under specific conditions could find application on a broad spectrum of different application, for example as optoelectronic device manufacture, as chemical sensors, as active as well as passive optical components.[2][3] In medicine nanotechnologies could be useful on many levels, from research to diagnosis and even therapy: micro and nanodevices, such as DNA or protein microarrays [4] and luminescent quantum dots [5] can help genomic and proteomic research and can be tailored for cancer diagnosis. Nanostructured materials can be used as drug delivery systems or as drug encapsulating ones, nanoparticles can work as gene vehicle instead of viruses, and nanoengineered materials can be implanted and promote tissue reconstruction.[1]
For what regards biomedical applications, nanotechnology should aim to produce devices displaying the following properties:

- very small dimensions and their dimensions and inner structure must be suitable to the biomolecule they are intended to interact with;
- ability of trapping and retaining high amounts of active biomolecules if they have to serve as sensors or carriers;
- biocompatibility, a general requirement for medical purpose produced materials.

It is clear that, besides nanomaterials production techniques, a leading role is played by surface modification techniques, which allow deposition of selective and bioreactive layers.
In particular in this work we studied nanostructured microparticles made of (luminescent and non-luminescent) porous silicon.
After the discovery of porous silicon by Uhlir[6], p-Si has been widely studied since the concern over possible toxicities of conventional metal-containing quantum dots have inspired growing research interests in colloidal silicon nanocrystals and silicon quantum dots. This is related to their potential application in a number of fields such as solar cells, optoelectronic and photonics devices, drug carrier and fluorescent bio-labeling agent[2][7][8]. Moreover their attractive properties, such as large surface area and pore volume, high

loading efficiency, biocompatibility, and biodegradability, make them versatile carriers for drug delivery and imaging applications.
Benefiting from these advantages, a wide variety of therapeutic and imaging agents have been successfully loaded into the p-Si carriers.

To fully exploit the p-Si potentiality, many parameters must be taken into consideration, in particular:

a morphological properties (surface area, free volume, pore size) to offer room for the cargo;

b chemical properties (surface reactivity and charge) to permit the covalent or electrostatic binding of the payload in addition to a favorable interaction with the body fluids;

c optical properties for in vivo monitoring.

The last two are the crucial points considering that in general the micro p-Si used for biological studies, after functionalization, has lost its light emission properties and must be labeled with organic dyes to follow its uptake by cells and distribution in tissues.[9][10] For these reasons during our thesis work we paid particular attention in making sure that the p-Si particles maintain a bright visible luminescence even after functionalization, in order to be able to follow them during their journey monitoring their luminescence directly without giving up on the several advantages that a particles coating with organic molecules could offer.

Finally a good drug delivery system requires not only a high loading capacity, but also the ability to retent and protect the loaded therapeutic agents within the porous nanostructure until it reaches the targeted sites in order to maximize their toxicity and avoid drug diffusion into healthy tissues.
The optimization of these properties should also take into account that the delivery system should present an environment suitable for the specific drug to be delivered and the ability to interact favorably with the biological fluids.

On the basis of the advantages offered by p-Si as drug delivery system, we aimed the present work at the design of an original strategy to obtain p-Si microparticles able to load a hydrophobic cargo (as many drugs currently used are) and presenting an external surface exposing hydrophilic groups negatively charged to increase the lifetime in biological fluids. To reach this aim we designed a procedure allowing a differential functionalization of the surface inside and outside the pores. This strategy was based on a liquid masking method [11] which allows the protection of the surface inside the pore while that outside the pores is selectively modified.
According to the designed procedure, we should obtain a bifunctional p-Si presenting hydrophilic external surface and hydrophobic inner pore walls, strongly luminescent and highly stable.
Beyond the set-up of this original functionalization method, an important task was the characterization of the material, before and after each functionalization step. The characterization of the starting porous silicon was performed with the aim of achieving the best

morphology of the porous structure (porosity, pore size and density).
The characterization of the material after each functionalization step was performed to check the morphology and the chemical composition of the surface. The following are the analysis that we performed:

- Photoluminescence Spectroscopy
- Raman Spectroscopy
- Fourier Transform Infrared Spectroscopy (FTIR)
- X-ray photoelectron spectroscopy (XPS)
- Contact angle

This thesis is structured as follows:

- **Porous Silicon and Surface Functionalization** is introductory and intended to give a brief overview on materials and methods used for surface modification and to present silicon properties underlining how useful they can be for biomedical applications;
- **Experimental Methods and Apparatus** presents the experimental work done in order to identify the best set-up of this original functionalization method, and to characterize the material;
- **Experiment: Methods and Results**, in this section the data analysis will be presented and discussed;
- **Conclusion**, in this section are summarized briefly the obtained results.

Chapter 1

Porous Silicon and Surface Functionalization

1.1 Porous silicon

Since it was discovered in 1956 by Uhlir [6], while performing electrochemical etching of silicon, a great number of investigations have been undertaken in order to understand and better control p-Si formation mechanism, the result of which revealed that p-Si is a large and morphologically rich labyrinth-like structure, with pores penetrating deep into the silicon volume (up to some tenth of microns) and separated by silicon walls maintaining the crystalline structure of the substrate. After the discovery that highly porous silicon presents an intense photoluminescence in the visible region even at room temperature, p-Si has continuously attracted the attention of the scientific community with an ever increasing number of applications.
Porous silicon reactive nature allows for selective formation of unique electronic components and mechanical nanostructures. In fact, its optical properties made it a versatile material for micro- and optoelectronic device manufacture,and a successful employment of p-Si in sacrifical/separation layers, in chemical sensors, in active as well as passive optical components has been reported.[4][12][2][3]

Due to the large pore surface area, an extreme reactivity, it has been founding successful applications as catalyst for chemical reaction occurring on its surface, and as a gas sensor(if a chemical modification of it surface is previously performed its optical properties varies as a response to inner environment variation)[7][8].
The attractive properties of p-Si nanoparticles, such as a large surface area and pore volume,high loading efficiency. biocompatibility and biodegradability make them versatile carriers for drug delivery and imaging applications. Benefiting from these advantages, a wide variety of therapeutic and imaging agents have been successfully loaded into the p-Si carriers, e.g. conventional drug molecules, peptides, small interfering RNA and quantum dots[13].[14][15][16] Moreover, luminescent porous silicon nanoparticles can be produced in order to be used as fluorescent probes allowing us to follow them during their journey. Furthermore they are less subjected to photobleaching in comparison to organic fluorescent probes and their surface can be modified in order to address nanoparticles toward different targets.

So, with the generic name of p-Si we can describe a huge variety of complex materials whose only common denominator is the fact that they are made of silicon and present a porous structure. Their properties (structural, optical, electrical, surface-related, mechanical) depend on many different parameters and can be tailored to apply for a huge amount of different applications.

1.1.1 Porous silicon Formation

Porous silicon (pSi) is formed by electrochemical anodic etching of Si in an HF aqueous solution. Following an electrochemical reaction, at the silicon surface a partial dissolution of Si takes place. Let us describe on the various factors which rule this process.

Current-voltage Characterization

A measurable current flows through the system when a potential is applied to the silicon wafer with respect to an electrode submerged into an HF solution. For any current to pass the Si/electrolyte interface, a change from electronic to ionic current must occur. Thus at the Si/electrolyte interface a specific chemical redox reaction must occur.
This means that a precise chemical reaction is induced when a specific potential is applied to the system, the nature of this reaction is fundamental to the formation of p-Si.[8]

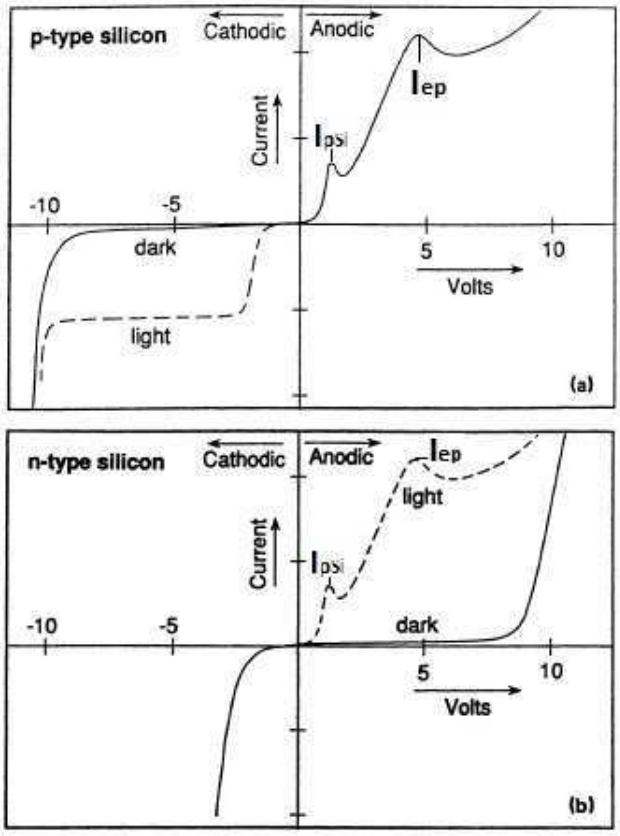

Figure 1.1: Typical i-V curves for p-type (a) and n-type (b) silicon.[17]

Figure 1.1 shows the "typical" i-V curves for n- and p-type doped Si in aqueous HF.[17][18]
The i-V curves show some similarities to the normal Schottky diode behavior expected for a semiconductor/electrolyte interface, but some important differences occur. The difference between p-type and n-type silicon resides in the majority carriers electrical charge(

holes for the former and electrons for the latter), while the chemical reaction at the interface remains the same (if the polarization and the current are the same) for both types.
For both n- and p-type materials, during cathodic polarization silicon is stable, electrons flow into the electrolyte and there is no change in the silicon surface structure. The only important cathodic reaction is the reduction of water at the Si/HF interface, with the formation of hydrogen gas. This usually occurs only at high cathodic overpotentials, also known as reverse breakdown.
Under anodic polarization holes flow into the electrolyte and the silicon dissolves into the electrolitic solution. The surface morphology is dominated by a vast labyrinth of channels that penetrates deep into the bulk of the Si. P-Si is formed.
At high anodic overpotentials there is an effect called electropolishing: The porous layer is formed and simultaneously removed from the substrate.[7] Pore formation occurs only in the initial rising part of the i-V curve, for potential value below that of the small sharp peak (see Figure 1.1). This current peak is called the electropolishing peak (I_{ps}) and separates the region of p-Si formation and of electropolishing.
Above the second maximum I_{osc} (see Figure 1.1) holes accumulation on silicon surface causes its electropolishing and produces a mirror-like silicon surface.
The quantitative values of the i-V curves, as well as the values corresponding to the first and second electropolishing peak, depend on etching parameters (electrolytic solution chemical and physical characteristics) and wafer doping. For n-type substrates, this typical i-V behavior is observed only under illumination because hole supply is needed.

Surface dissolution chemistry

The formation process of p-Si is a very complex function of numerous factors, for this reason many theories have been proposed on the various mechanisms of formation and morphology of p-Si.
After all it is generally accepted that: defect sites on silicon surface are involved in the initiation of pores (because current density is locally higher near them), while pore growing process and final diameter, density and pore wall thickness are determined by the properties of silicon and by the anodization conditions.
Among all the chemical dissolution mechanisms proposed, the most accredited is the one proposed by Lehmann and Gösele [19], described in Figure 1.2

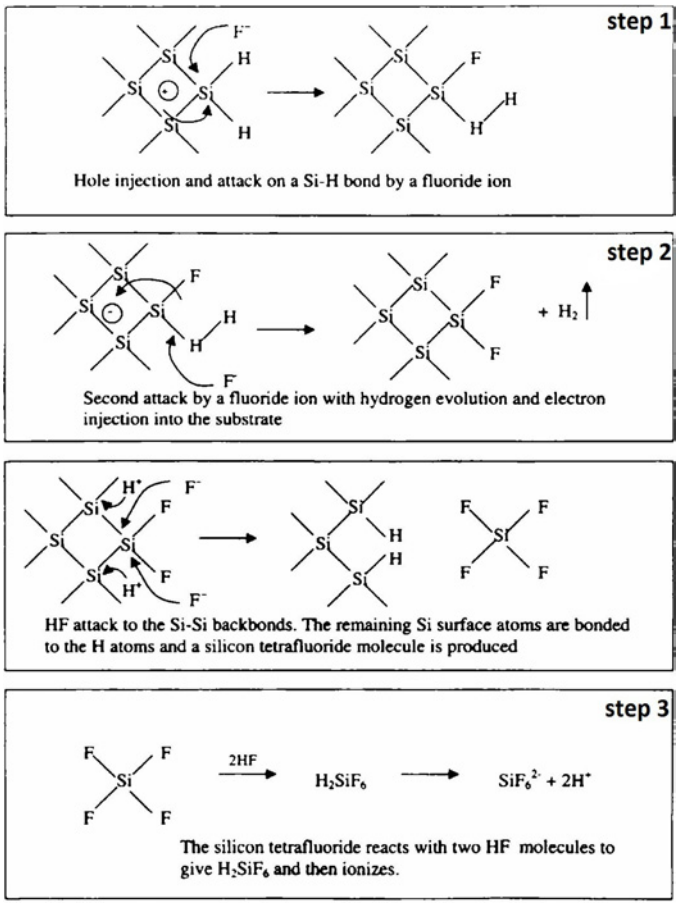

Figure 1.2: Lehemann and Gösele's model mechanism for the chemical dissolution of silicon in HF solutions leading to p-Si formation.

In their scheme, if a hole (h+) reaches the surface nucleophilic attack on Si-H bonds by fluoride ions can occur and a Si-F bond is established (step 1 in Fig. 1.2). Due to the polarizing influence of the bonded F, another F- ion can attack and bond under generation of an H, molecule and injection of one electron into the electrode (step 2). Due to the polarization induced by the Si-F groups, the electron density of the Si-Si backbonds is lowered and these weakened bonds will now be attacked by HF or H_2O (step 3) in a way that the silicon surface atoms remain bonded to hydrogen. If a silicon atom is removed from an atomically flat surface by this reaction, an atomic size dip remains. This change

in surface geometry will change the electric field distribution in such a way that hole (h+) transfer occurs at this location preferentially. Therefore, surface inhomogeneities are amplified. It has been shown that pores of about 1 pm will establish in a few minutes on polished n-type silicon surfaces by this process.[20] If the walls between the pores are depleted of holes (h +) they will be protected against dissolution.
Hole near the surface are required because they can induce a polarization on the otherwise nonpolar Si-H bond, thus allowing its nucleophilic attack by a F^- ion. During the pore formation two H atoms evolve for every Si atom dissolved. The H evolution diminishes when approaching the elettropolishing regime and disappears during electropolishing. Current efficiencies are about four electrons in the electropolishing regime.
The global anodic semireactions can be written during pore formation as:

$$Si + 6HF_2SiF_6 + H_2 + 2H^+ + 2e^-,$$

and during electropolishing as:

$$Si + 6HF_2SiF_6 + 4H^+ + 4e^-.$$

The final and stable product for Si and HF is in any case H_2SiF_6 or some of its ionized forms. This means that during pore formation only two of the four available Si electrons participate in the interfacial charge transfer while the remaining two undergo corrosive hydrogen liberation. In contrast, during electropolishing, all four electrons are electrochemically active.
Besides this main electrochemical dissolution, a parallel slow dissolution takes place: p-Si undergoes a rapid oxidation in solution and thus oxide layer is instantly removed by Hf present in the solution itself. This chemical dissolution rate depends on etching solution pH and tends to fasten up as OH^- ions concentration grows.

Pore formation

While it is generally accepted that pore initiation occurs at surface defects or irregularities, different models have been proposed to explain pore formation in p-Si.
Some basic requirement have to be fulfilled for electrochemical pore formation to occur [21][22][23][20]:

- Holes must be supplied by the bulk and be available at the surface.

- The pore walls have to be passivated, while the pore tips must be active in the dissolution reaction. Therefore, if a surface is depleted of holes it is passivated to electrochemical attach.
  Hence the electrochemical etching is self limiting and hole depletion occurs only when every hole that reaches the surface reacts immediately. The chemical reaction is not limited by mass transfer in the electrolyte.

- Pore walls, depleted of holes, do not dissolve during anodization and dissolution proceeds at pore tips. Pore wall carrier depletion is thus confined by the high resistivity.

- The current density should be lower than the electropolishing critical value.

For current densities above such value, the reaction is under ionic mass transfer control, which leads to surface charge of holes and to a smoothing of the Si surface(electropolishing). The behavior at high current densities turns out to be useful to produce p-Si free-standing layers. Raising the current density above the critical value at the end of the anodization process results in a detachment of the p-Si film from the Si substrate.
In the low current density regime, where p-Si forms, some considerations apply [7][23]:

- A surface region decreased of mobile carriers is formed at the Si/electrolyte interface. This region is highly resistive (in comparison to bulk Si). The thickness of the depleted region depends on the doping density. It is several μm thick for lightly n-type doped Si. It is thin for highly n- or p-type doped Si, and it does not exist for lightly to moderate p-type doped Si.

- The size of the pores is related both to the depletion layer width and to the mechanism of charge transfer.[24]

- In highly doped substrates charge transfer is dominated by tunneling of the carriers, and the pore size reflects the width of the depletion region, being typically around 10 nm.[25]

- In lightly doped n-type Si anodized in the dark,generation of carriers occurs at breakdown. The pore dimensions are about 10-100nm (mesoporose), regardless of doping density. Under illumination the pore size is dependent on doping density and anodization conditions with diameters in the range 0.1-20μm (macropores).[25]

- A hole depletion is expected in any case if the dimension of the nanocrystals are about a few nm, independently of the substrate type and doping. In this size region, quantum confinement is effective and the Si band gap is increased. A hole

needs to overcome an energy barrier to enter this region. This is highly improbable. The quantum confinement is responsible for pore diameter below 2nm, denoted as nanopores. Nanopores can be found on every type of p-Si sample, but only in moderately and lightly p-type doped substrates does pure nano p-Si exist.[8]

- Both mechanisms coexist during p-Si formation, resulting in a superposition of micro and meso structures, whose average size and distribution depend on substrate and anodizing conditions.[25]

Etching parameters influence on p-Si formation

Pore dimensions and density are determined by two groups of factors: those affecting carrier density on the surface of a pore (including doping type and concentration, potential and illumination) and those that affect only the distribution of the reaction (including current density HF concentration and illumination frequency and intensity).

Current density and HF concentration influence p-Si porosity (defined as the void volume percentage within p-Si layer): for a given HF concentration, porosity grows as current density grows, while, for a given current density, porosity grows with decreasing HF concentration [7]. Low HF concentration can also lower down I_{p-Si} value and thus lower down the limit of electropolishing current conditions.

Doping influences pore morphology and dimensions. In p-type silicon pore diameters and pore wall thickness both increase with increasing doping level (i.e. with decreasing resistivity). Porous structure is very homogeneous for low doping, while for high doping levels pores develop along preferential directions and homogeneity is diminished. In n-type silicon, pore diameters and interpore spacing are generally higher and decrease with increasing doping levels.

Light promotes the formation of porous silicon starting from n-type silicon, but light with wavelength shorter than 700 nm can increase porosity and reduce pore wall thickness in p-type made p-si too. Dissolution is enhanced by photogenerated holes which made the bulk silicon dissolution possible.

Electrochemical solution temperature can influence crystallinity grade of obtained p-Si and its luminescence characteristics.

The applied potential and current density control the dissolution, but the same thing is valid for current density. Generally is desirable to work with constant current rather than constant voltage, because under these conditions we obtain a better control on porosity and depth of the final porous silicon product.
Since, a modulation of the current applied results in a change of the microstructure and porosity of p-Si, it can be used to tailor the growth direction of the pores, making it one of the most influential parameters.

Chemical composition of the etching solution. Due to the hydrophobic character of the clean silicon surface, absolute ethanol is usually added to the aqueous HF solution to increase the wettability of the PS surface and to improve the uniformity of the PS layer depth. In addition, during the reaction there is H_2 evolution. Bubbles form and stick on the silicon surface in pure aqueous solution, whereas they are promptly removed if ethanol or some other surfactant is present. Moreover, it has been found that lateral inhomogeneity and surface roughness can be reduced (increasing electrolyte viscosity) either by diminishing the temperature or introducing glycerol in the composition of the HF solution[21].

Drying of sample is a critical step since it introduces a large capillary stress. The decrease of pressure within pores,associated with the evaporation of the electrolyte from the pores, can result in extended cracking of porous structures, in particular on highly porous layers. Pentane drying is the easiest method to reduce capillarity stress. Pentane has a very low surface tension and, as the decrease of pressure within pore is proportional to the filling liquid surface tension, a final rinse in pentane leave p-Si layer undamaged.

P-Si structure and chemical composition

Many techniques(TEM,X-ray diffraction, FTIR etc.) have been exploited to characterize p-Si structure and surface chemistry and now p-Si can be described as an interconnected web crystalline silicon wire, maintaining the same crystallographyc orientation as the original bulk silicon, separated by pores with variable dimensions. On oxidized p-Si the presence of nanosized crystals dispersed into an amorphous porous matrix is observed.
The chemical composition of p-Si surface depends on its history. P-Si surface is highly reactive: just after electrochemical etching it is hydrogen terminated, but soon a process of aging establishes, in which hydrogen atoms are progressively and differentially replaced by oxygen.
Slowly, an amorphous superficial layer, whose chemical structure is made up by $Si - O_x$ ad $Si - H_x$ groups, grows on. The interface between crystalline p-Si structures and the amorphous layer can present many defects (dangling bonds) that can strongly influence p-Si luminescence. Beside oxygen, p-Si can absorb other impurities from external environment, above all carbon compounds.
Many different factors can determine p-Si properties: the presence of 2D or 3D spatially confined silicon structures, amorphous regions with different chemical composition, a large and very reactive inner surface whose chemical composition changes with time (and surface role can be of paramount importance in structures where a high percentage of constituent atoms are located on it).[21]

1.1.2 Photoluminescence process

Porous silicon is an efficient light emitter even at room temperature and this property strongly distinguish it from the bulk material from which it is obtained.
Silicon, in fact, presents a very low emission quantum yield at room temperature (about one emitted photon every 10^7 electron-hole pairs previously generated), due to its indirect band gap, which implies that electron-hole recombination processes must be phonon assisted.[8]
For a moderately doped silicon sample at room temperature, radiative lifetime can be of the order of some ms since these multiple bodies events have low probability and extremely low rates.
Due to very long radiative recombination times, charge carriers prefer to recombine through competitive non radiative processes characterized by shorter lifetime (about ns). Non radiative recombinations take place thank to energy levels associated to defects or impurities present in the semiconductor sample or on its surface.
P-Si is a material where radiative recombination processes have been made efficiently competitive with non radiative ones.
To explain this phenomenon, many different models have been presented, among which the most accredited is that of quantum confinement.

The quantum confinement model

According to this model, p-Si photoluminescence is due to carriers confinement within low dimensionality system that compose p-Si structure.
When charge carriers are confined within regions where all three or only two dimensions have smaller size than the Bohr radius of the exciton in silicon(4.9nm) we talk about systems called "quantum dots" or "quantum wires" respectively.
Carrier confinement leads to an energy level quantization, both in the valence and in the conduction band (similarly to what happens for a particle confined within a potential well). This confinement causes a shift of the conduction band and thus of the energy minimum (E_c) toward higher energies. Conversely the valence band and the energy maximum (E_v) are shifted toward lower energies, causing a widening effect of the band gap.
This effect become increasingly important as the silicon nanostructures lowers. In particular as the silicon dimensions decrease the the enlargement of the band gap increases. Thus the minimum energy required to generate an electron-hole pair becomes higher when the dimensions of the nanostructures decrease.
Then, whereas bulk silicon displays an emission band in the near IR centered at 1.17 eV (that is the band gap for an infinite silicon sample), p-Si and silicon nanocrystals display emission spectra shifted toward higher energies (1.4-2.2 eV) and tunable in the whole visible range just by varying the nanostructures size.
The quantum confinement effects increase when the number of involved dimensions increases.
The quantum confinement of charge carriers is also responsible for the PL quantum efficiency improvement(with respect to bulk silicon), for three reasons:[26]

1. due to the better superposition in the electron and hole wavefunction, caused by their spatial resolution, quantum confinement causes an increase in the exciton bind-

ing energy.
As a matter of fact, in bulk silicon exciton binding energy is very similar to thermal energy and this implies that the probability for the two charge carriers of being set apart, before they can radiative recombine, is high. At the same time if the electron and hole move far away from each other, the probability for them to recombine in non radiative ways after reaching the surface or a bulk defect is enhanced.
This is why at room temperature bulk silicon is a good photon absorber, but a bad emitter.
Conversely in p-Si the enhanced exciton binding energy make the two carrier energy stable for periods long enough to allow them to recombine through indirect radiative ways.

2. Quantum confinement enhances the probability for direct radiative transition to take place.
Charge carriers spatial confinement determines a widening of their corresponding reciprocal space wavefunctions and a consequent improvement in the probability of radiative transition which do not need to be phonon assisted.
A widening in the reciprocal space electron and hole wavefunctions determines a larger superposiotion and using a first order theory we can predict the probability of a direct transition.
This effect is important above all for nanostructures smaller than 2.5nm: for them,radiative lifetime results shorter than $10\mu s$ and they display intermediate properties between direct and indirect band gap materials.

3. Quantum confinement within very small volumes decreases the probability for exciton to find volume defects that can act as non radiative recombination centers. This prevents the quenching effect of the luminescence due to the fact that radiative recombination is more efficient than non radiative one.
Nanostructure sufficiently small can eventually present no defects at all and electron and hole can recombine radiatively within some μs.

For all this reasons p-Si has a good PL efficiency, more than four orders of magnitude higher than that of bulk silicon.

Other methods

Even if quantum confinement is nowadays considered the best model to explain p-Si and silicon nanocrystals optical behavior, a variety of other theories have been proposed stressing the importance of other parameters in order to understand silicon photoluminescence ability.
In particular some experimental results seem to stress the importance of surface oxidation or chemical composition. According to other models, luminescence could originate from polysilanes and siloxanes present on p-Si surface, or could e associated to the trapping of carriers near bulk silicon defects or at the Si/SiO_2 interface for aged p-Si.
A "surface state" [27] model has also been proposed, according to which, in silicon nanostructures adsorption is related to quantum confined system, while emission can be originated from localized surface state with energies inferior to p-Si band gap.
Within a silicon nanocrystal electron and hole can radiatively recombine through three different processes:[26]

1. electron and hole can recombine without involving surface states. In large crystallites, phonons are required for this kind of recombinations to take place, while they are not strictly needed in smaller nanostructures. These recombinations have however a low probability with respect to non radiative ones.

2. One of the two carriers is trapped near a low energy surface state and recombines with a delocalized carrier. This band-to-localized-state transition characterizes processes involving surface states and is rapid.

3. Both carriers are confined within a low energy surface state and recombine through a tunneling process, so this transition is slower than the preceding one.

The hierarchy of transition processes proposed by this model could explain the existence of different emission bands for p-Si and strong Stokes shift between absorption band gap and emission energies observed for this material, and takes into account the importance of nanostructures surface chemistry (which can influence the energies of localized surface states). So both bulk phenomena (quantum confinement) and surface related ones (localized surface state related to oxidation, impurities, amorphous regions) must be involved in absorption and emission processes in p-Si. The influence of surface related processes on p-Si luminescence has been largely studied above all for what regards surface oxidation. Many oxidation techniques (thermal, anodical, chemical oxidation) have been applied to p-Si, above all in order to stabilize its PL characteristics and, in general, they succeed in enhancing emission efficiency and stability, but even strong oxidation can not prevent contaminating agents to penetrate in a still porous material, and more specific surface modification must be taken into account in order to optimize p-Si for different applications.

1.2 Hydrosilylation

The majority of the methods known to functionalize porous silicon surface involve directly binding of organic molecules onto freshly etched H-terminated p-Si surface. For example those exploiting -OH groups of carboxylic acid or alcohols are based on the breaking of surface Si-Si bonds, promoted by light in reversed bias conditions or by temperature, and binding organic molecule by Si-O-C bridges.
Hydrosilylation (also known as Alkylation when alkyl chains are introduced on Si surface), instead, leaves untouched Si-Si bonds and forms Si-C links by breaking Si-H surface bonds. Hydrosilylation implies that the molecule to be grafted onto Si surfaces has at least one double or triple bond between carbon atoms, as the reaction proceeds via a radical chain mechanism triggered by breaking of Si-H linkage and the production of Si• radicals on the surface.[28]
These radicals are the binding sites for alkenes and alkynes, as shown in Figure 1.3

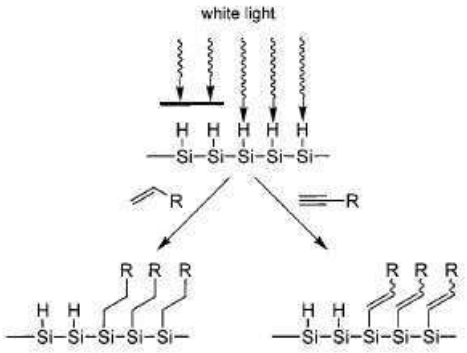

Figure 1.3: Schematic illustration of liquid masking method for selective chemical modification of porous Si films[1]

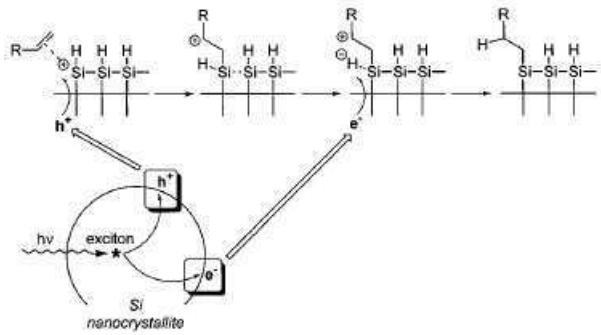

Figure 1.4: Schematic illustration of liquid masking method for selective chemical modification of porous Si films[1]

The creation of Si• can be promoted by high temperatures, by UV or white light illumination (see Figure 1.4) or by using catalysts such as Lewis acid Ethyl Aluminum Chloride ($EtAlCl_2$) and the formation of Si-C bonds on the surface is reported to enhance silicon stability against oxidation. Of course, free oxygen should be avoided during

hydrosilylation because it can be a competitor to the organic molecule during radical reaction, above all in wet environment and at high temperature.
So, whereas oxidation was required for silanization, hydrosilylation does not need to spend time for oxydation procedures, as it must be done under inert atmosphere (for example in deoxygenated organic solvents). Not only aliphatic or aromatic alkenes or alkynes can be grafted onto silicon nanostructures surface by hydrosilylation, but also molecules bearing functional groups displaced from $C = C$ or $C \equiv C$ bonds, such as, for example, carboxylic acid [29], allowing one to tailor originally hydrophobic surface to be hydrophilic and suited for successive macromolecules binding.

Chapter 2

Experimental Methods and Apparatus

As described in the Introduction we designed a strategy for differentially modifying the inner/outer pore surface in luminescent porous Si particles which are highly biocompatible and biodegradable. To obtain a selective functionalization of the inner and outer surface of the drug delivery porous system, we adopted a liquid masking method[11]. The procedure foresees the followings 5 steps of surface modification summarized in Figure 2.1.

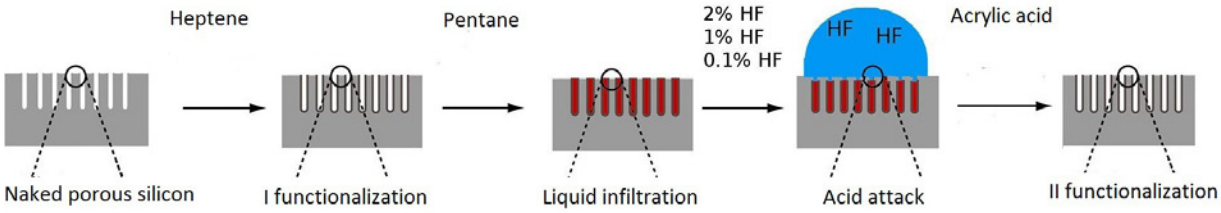

Figure 2.1: Schematic illustration of liquid masking method for selective chemical modification of porous Si films[1]

A **Freshly etched porous Si thin film:** Porous silicon(p-Si) used for this work was prepared by electrochemical etching and presents hydride species throughout the inner and outer pore surfaces.

B **First Photopatterned Hydrosilylation:** The nucleophilic attack on silicon leaded to the formation $Si-CX$ bonds ($Si-CH_2$ and $Si-CH_3$ or $Si-CBr$) and a carbocation stabilized by a $\beta-silyl$ group. The acidic carbocation intermediate abstracts a hydride from an adjacent Si-H bond to yield the neutral organic termination.

C **Infiltration:** the functionalized p-Si was submerged in an inert organic liquid (pentane) which penetrated the pores protecting the pore walls.

D **Acid Attack:**the pentane-infiltrated sample was then immersed in aqueous HF solution; the interior of the porous structure is protected by the presence of the hydrophobic liquid mask and the acid only interacts with the exposed surface of

porous silicon generating a hydrogen terminated outer layer by removing the alkylic chains.

E **Second Photopatterned Hydrosilylation:** The procedure used in this case is equal to the one described in point B) the only difference is that we hydrosilylated using acrylic acid producing Si-COOH bonds. The resulting material is a bifunctional p-Si presenting hydrophilic external surface and hydrophobic inner pore walls, strongly luminescent and highly stable.

Beyond the set-up of this original functionalization method, an important task was the characterization of the material, before and after each functionalization step. The characterization of the starting porous silicon was performed with the aim of achieving the best morphology of the porous structure (porosity, pore size and density). The characterization of the material after each functionalization step was performed to check the morphology and the chemical composition of the surface. The following are the techniques that we used:

- *Photoluminescence Spectroscopy:* it provides an optical characterization of the material, since PL peak position strongly depends on p-Si porosity. It can also be used as a parameter for choosing the starting material rather than for post production characterization;
- *Raman Spectroscopy:* it provides a chemical characterization of the sample and allows also a cross sectional analysis of the chemical groups grafted on the surface;
- *Fourier Transform Infrared Spectroscopy (FTIR)*: it gives a chemical characterization of the material, but without distinguishing between the inner and the outer surface. Consequently it provides a value mediated over the sample volume under the light spot;
- *XPS:* measures the elemental composition of the Si layer surface and produces a quantitative spectroscopic result. The XPS spectra were acquired at different tilting angles to obtain the surface composition profile along the p-Si pores;
- *Contact angle:* gives an information on the wettability of a solid surface by a liquid, providing a mean characterization of the physical proprieties of the surface leading to some information about the chemistry of the surfaces.

2.0.1 Naked porous silicon

Porous silicon used for this work has been prepared by electrochemical etching in a custom made Teflon cell in which the silicon wafer was kept in contact with the positive electrode by its aluminum implanted back surface while the front surface was in contact with an electrolytic HF solution.[6] A platinum counter-electrode, facing the silicon surface, was dipped into the solution. The current for the electrochemical process was supplied by a controlled generator.

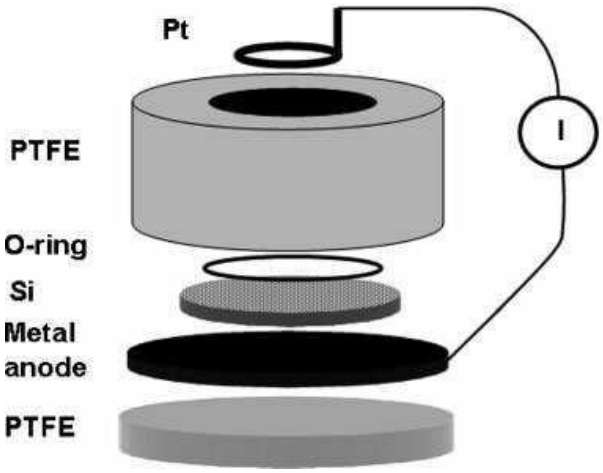

Figure 2.2: Scheme of an anodization cell.

The first stage of my work consisted in the investigation of the proper type of silicon, etching condition and chemicals useful in order to obtain starting materials presenting the proper characteristics suitable for our purposes and, at the same time, presenting features suitable for the analysis procedures of interest. For this reason we tested different types of silicon doping and together we varied the etching solution and the current intensity to probe a vast spectra of possibility in order to select the best settlement.
In principle our aim was to obtain luminescent p-Si microparticles. However, some of the characterization techniques (surface analysis by microRaman) are disturbed by PL emission. Moreover, the experiments aimed at the characterization of the profile of the chemical groups along the pores, required a porous layer thicker more than 5μ in order to be able to distinguish in cross section between the bottom of the pores and the top of them. In this case we used a micro p-Si, obtained by a slightly different etching procedure which pore depth was approximately 10μ and did not emit PL. We are well aware that by changing the etching conditions the morphological characteristics of the p-Si layer are modified. However, we used microRaman to test the chemical modification of the p-Si surface. We can reasonably assume that the surface chemistry is only marginally affected by the p-Si morphology.

Luminescent silicon

Porous silicon photoluminescence(PL) presents the following main characteristics:

- The PL emission lineshape is a gaussian curve;
- PL peak position strongly depends on p-Si porosity, this peak shift toward higher energies as porosity increases (the thickness of mean interpore crystalline walls decreases)
- as the p-Si age in air, the PL intensity varies and the peak position shifts towards the blue. This shift reaches a stability in a characteristic period of time typical of the functionalization and the material itself. It is imputable to oxidation.

Since it is well documented that a relatioship between PL emission wavelength and crystallite size exists [30][31], we can use the peak PL emission to estimate the size of the crystallites.

The optimum etching conditions were found after several experiment trials. The most significant results of these trials are reported in Appendix A

The final etching procedure contemplate:

- *Silicon:*p-type,boron doped resistivity:$10 - 20\Omega \cdot cm$, $< 100 >$ oriented;
- *Electrolytic solution:*16% hidrofluoric acid in Ethanol;
- *Current density:* $70mA/cm^2$ for $15min$.

The samples were used as porous layer on bulk crystalline silicon or as micro p-Si powder, depending on the analysis we performed.

Thus depending on the case we added two different possible last step:

1. *Powder:* the porous layer was scratched from the wafer using an cutter in order to obtain a p-Si powder and then collected in a toluene solution saturated with nitrogen and afterwards sonicated at 400W for 5min.
2. *Porous silicon layers on bulk silicon:* the freshly etched silicon porous layer, transferred into a baker, immersed in toluene and kept in a nitrogen saturated environment.

In table 2.1 we present the characteristics of the resulting materials, in this section we provide just an overview on the main properties. The detailed characterization is reported in "Appendix A".

PL	Size	Thickness	Porosity	estimated pore size
$(719\pm5)nm$	$(13 \pm3)\mu m \times (4 \pm 2)\mu m$	$(44 \pm2)\mu m$	(77±3)%	25nm

Table 2.1: Most relevant morphological characteristics of p-Si powder and layer.

As previously mentioned this kind of material was used for: PhotoLuminescence, Fourier Transform Infrared Spectroscopy and contact angle measurements.

Non luminescent silicon

This material was used for the characterization of the chemical groups presents on the surface by microRaman and X-rays photoelectron spectroscopy. For this reason the samples were prepared in the form of porous silicon layer still attached to the wafer bulk. These types of analysis are really affected by photoluminescence since the first one is based on the collection and analysis photoelectron emitted from the parent atom after the sample surface was irradiate with a soft (low energy) X-ray, while the second explore shift in energy after the laser light had interacted with molecular vibrations, phonons or other excitations in the system.

For this reason we have selected a material almost completely black and at the same time thick enough for Raman spectroscopy.

The final material and etching conditions:

- n-type silicon wafer, anthimony doped resistivity: $0.01\Omega \cdot cm$, orientation: $< 100 >$,
- current density: $5mA/cm^2$ for $30min$.

In table 2.2 we present the characteristics of the resulting materials. As for the previous case the detailed characterization is reported in "Appendix A".

Thickness	Porosity	Estimated pore size [20]
$(44 \pm 5)\mu m$	$(77 \pm 3)\%$	20nm

Table 2.2: Most relevant morphological characteristics of p-Si powder and layer.

As for the luminescent preparation all the detail are reported in the "Experiment:Analysis and results" chapter and here we present a general view on the morphological characteristics of the resulting material.

2.0.2 First Photopatterned Hydrosilylation

In this section we are going to present the experimental detail used to functionalize our materials, a more specific description of the chemical reaction is provided in the "Porous Silicon and Surface Functionalization" Chapter.
Again, on the base of the characterization to be performed, we decided to use two different chemicals for our functionalization.
This kind of functionalization is appropriate for: FTIR, PL and contact angle.
Hydrophobic alkenes were grafted to the surface of porous silicon by a light or UV-light catalyzed hydrosilylation reaction.[32] Usually, the grafted alkene was heptene. In the case of the samples used for XPS characterization, 11-bromo-1-undecene was used instead of alkene since the bromine atom present in this organic compound gives rise to a characteristic XPS signals. Moreover, since bromine is rather uncommon as environmental contaminant, the grafted molecules containing bromine are well distinguishable from the organic surface contaminants. Also present a strong Raman peak at 647 cm^{-1}.[33]

The experimental details of the procedures used to functionalize the p-Si layers or the micro p-Si powders were slightly different, in order to be applied to the two different sample types.

Porous Silicon Powder

Heptene (11-bromo-1-undecene) was added to the mixture of freshly etched porous silicon particles (around 15 mg) and 10 ml toluene, at the final concentration of 1.6 mM (0.4 mM). The solution was then transferred into a glass balloon, connected to a condenser and a magnet was introduced inside the mixture.
The solution was kept under magnetic stirring with the aid of a magnetic stirrer placed under the balloon and the solution was refluxed for two hours at RT under nitrogen atmosphere and continuous magnetic stirring. [6]

The reaction took place under white-light illumination (250W led lamps) for luminescent silicon. While we were forced to use UV light for the n-type silicon.
The samples were then transferred into a glass vial and centrifuged for 8 to 15 min at 150g; the supernatant was collected and the micro p-Si powder was resuspended in pentane. the washing step with pentane was repeated 5 times, then the powder was collected and dried under nitrogen.

Figure 2.3: Hydrosilylation system.

Porous Silicon thin layer

Again also for this kind of preparation we used a 15ml toluene and Heptene (11-bromo-1-undecene) 1.6mM (0.4mM) solution in which the porous silicon wafer was dipped. Unlike the porous powder in this case was impossible to add a magnetic stirrer so we preceded to manually agitating the solution every 20 to 30 min.
The solution took place at room temperature(around $25°C$) under continuous nitrogen flux for 2hour.
Since the porous layer was still attached to the wafer, making it easier to handle, after the functionalization the sample was simply removed from the toluene solution and rinsed in pentane, then dried under N_2.

2.0.3 Infiltration

After the first functionalization step the samples were submerged in pentane for 2 min in order to make sure that it infiltrates the pores.
We chose to use pentane since it is insoluble in water, it easily enters the pores and evaporates at room temperature so it is easy to be removed from the outer surface of the material, making it the best choice for the liquid mask role.

2.0.4 Acid Attack

As for the previous cases two different procedures were applied to PSi powders and pSi layers in order to perform the acid attack properly.

Porous Silicon Powder
About 10 mg of pentane-infiltrated pSi powder were suspended in 1 mL of HF aqueous solution (0.1%, 1% and 2%) for 30sec, after they were centrifuged at 0.198g for other 30 sec. The supernatant was then replaced with pentane and centrifuged again at 0.198g for 10min, the procedure was repeated 5 times and afterwards the sample was finally dried under nitrogen flux.

Porous Silicon thin layer
In this case the wafer was simply transferred into a teflon plate then submerged in an aqueous solution containing a variable concentration of HF (0.1%, 1% and 2 %) for 1 min. As always it was rinsed in pentane and dried under N_2.

By this procedure the outer silicon layers should be removed as SiF6 and as a consequence the organic coverage is detached. After this reaction the outer surface of the nanopores should expose SH terminations.

2.0.5 Second Photopatterned Hydrosilylation

The second hydrosilylation step was performed using acrylic acid . Acrylic acid binds to the Si-H groups according to the mechanism reported in section 1.2 using the C-C double bond[34], and exposes a carboxylic functional group. This group is highly polar and negatively charged in aqueous solution at pH ≥ 4.

As for the previous cases we have to distinguish between the procedures of functionalization for powder and porous silicon layer.

Porous Silicon Powder

The p-Si powder was refluxed in 10 mL toluene containing 50 mM acrylic acid for two hours at RT under white light illumination, vigorous stirring and continuous nitrogen flux.

The solution was kept under stirring with the aid of a magnetic stirrer placed under the balloon and the samples were refluxed into the solution The samples were then transferred into a glass vial and centrifuged for 8 to 15 min at 150g; after that the supernatant was substitute with pentane. The procedure was repeated 5 times, changing the pentane after every centrifugation, and finally dried under N_2.

Porous Silicon thin layer

Again also for this kind of preparation we used a toluene and Heptene (11-bromo-1-undecene) 1.6mM (0.4mM) solution in which the porous silicon wafer was dipped. The reaction as performed as reported for p-Si powder except that only a gentle manual stirring was applied every 20-30 min since magnetic or mechanical stirring could damage the fragile p-Si layer. After two hours, the sample was removed and rinsed with pentane several times and finally dried under nitrogen.

Chapter 3

Experiment:Analysis and results

In the following sections I describe the experiments performed to characterize the samples after all the functionalization steps. To make the presentation clear, the data are grouped according to the experimental technique utilized to characterize the samples.

3.0.6 Photoluminescence Spectroscopy

In this section we reported the data concerning the PL emission by p-Si and p-Si powder after each functionalization step. In our work we wanted to prepare a porous material luminescent enough to be used not only as a drug loading system, but also as a fluorescent probe in order to be able to follow it during its journey. For this reason we put particular interest in checking the photoluminescence ability of our sample after each functionalization step, paying particular attention on the final product.
For our aim it was of fundamental importance that the luminescence of the end product would be: stable (after a first decay) enough to be applied in a practical use for in vitro simulations, intense enough to be easily detectable and also and also emitting in the red range of the EM spectrum.

Data collection
Florescence spectra of micro p-Si particles were obtained using Varian Cary Eclipse Fluorescence Spectrometer (Image 3.33).

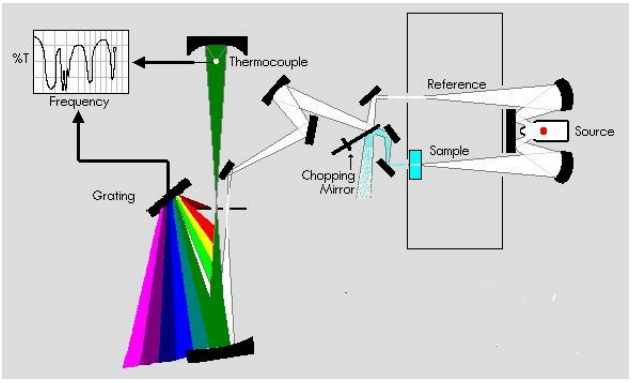

Figure 3.1: Varian Cary Eclipse Fluorescence Spectrometer working scheme.

The photoluminescence was tested using a 300nm or 350nm exciting light, with both emission and excitation slit at 10nm this allow us to reach a resolution of 5nm.
After each functionalization step, 1 mg of pSi powder was suspended in 2 mL toluene in a quartz cuvette

These measurements were performed to investigate the effect of the various functionalization steps. In some cases the PL decay over time was monitored, to investigate the modification of the PL with time. In fact, the p-Si utilized for this work presents a broad emission band in the red-infrared region. The p-Si aging induces a progressive shift of the emission peak toward the blue [35].

Data analysis

This kind of p-Si has a very large emission band raging from red to near-infrared light that shifts toward the blue as the sample ages.[36][37]
We studied this aging process by making an acquisition right after the sample preparation(0 hours) and at different times until 220-400 hours depending on the sample. At each time acquisition we collected 5 spectra and from a gaussian deconvolution we obtained the values of the peak wavelength and intensity.
Subsequently the results were averaged and reported in figures below.

Naked porous silicon

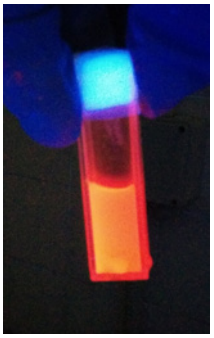

Figure 3.2: Photoluminescence of 1mg naked micro-pSi suspended in 2ml toluene.

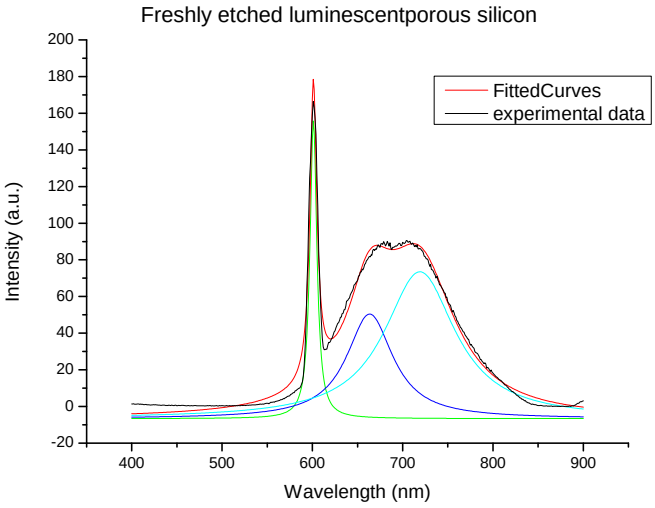

Figure 3.3: Photoluminescence of 1mg naked micro p-Si suspended in 2ml toluene.
the green and blue traces are the single curves of gaussian deconvolution, while in red is presented the final fitting curve, the black line is the experimental trace.

In Figure 3.3 is clearly visible the presence of two distinct red band emissions, properly described through the gaussian deconvolution. As we have previously seen the emission wavelength is strongly linked to the silicon morphology suggesting the presence inside the sample of two different family of silicon nanostructures.
The results of the gaussian deconvolution are the following:

- $\lambda = (719 \pm 5)nm$ and $I = (89 \pm 6)a.u.$

- $\lambda = (663 \pm 5)nm$ and $I = (84 \pm 5)a.u.$

The two components are competitive and the color of the resulting sample is a combination of the two contributions(Fig.3.2).

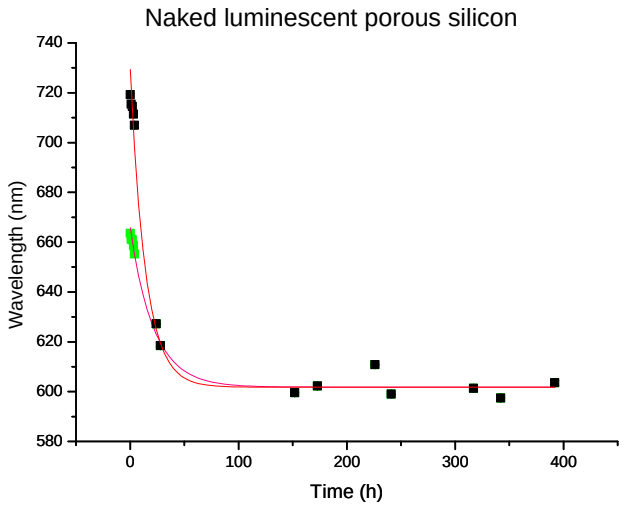

Figure 3.4: Time dependance emission wavelength of 1mg of naked micro p-Si suspended in 2ml toluene. In black is reported the aging process of the band with the higher starting wavelength, the green points represent the aging history of the band with the lower starting wavelength. The red and purple curves are the exponential fit relative to the two different family. The errorbars are inside the dots.

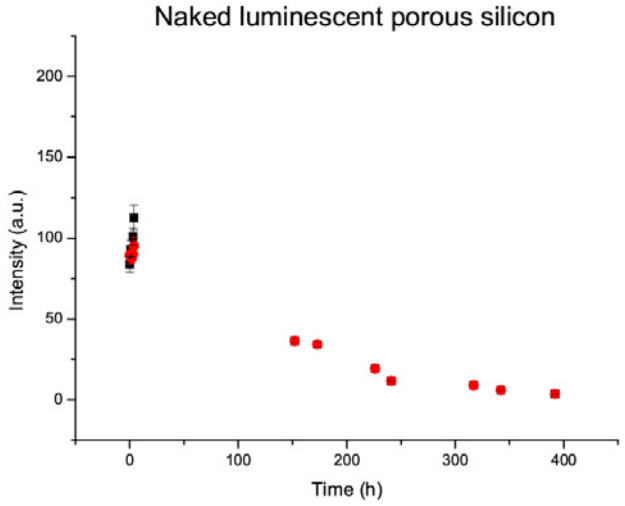

Figure 3.5: Time dependance of the PL intensity of 1mg naked micro p-Si suspended in 2ml toluene. In this case the red dots correspond to the band with the higher starting wavelength, while the black ones are relative to the band with the lower starting wavelength.

In Figure 3.4 we can see that after less then 24 hours the double band disappeared, indeed the green and black data series, representing the two different evolution of the two red bands, merged into one. The same behavior is visible in Figure 3.5.
This fact led us to think that this behavior was due, not to the presence of two different types of nonostructures, but to the presence, inside our samples, of material with different

aging history. This is in good agreement with the preparation procedure of the starting material, indeed in order to be able to collect enough material for our analysis we performed two subsequently etching procedure, than the first obtained sample started the aging process half an hour before the second.
Since the aging effect causes the band to shift towards the blue in the EM range we decided to use the spectra whit the higher starting peak wavelength as reference to calculate the time constant of the process. Since the blue shift is described by an exponential decay: $\lambda = A_0 \cdot e^{-t/\tau}$, from the data fit we extrapolate $\tau = (16 \pm 2) hours$.
The luminescence emission within the limits of our analysis seems to reach a plateaux after approximately 30 hours as the wavelengths of the peak emission approaches $\lambda = (601 \pm 5) nm$ (Fig.3.4)

Porous silicon functionalized with Heptene

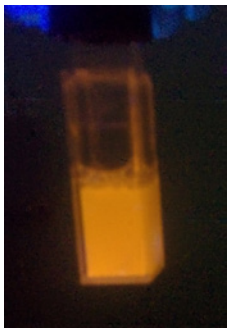

Figure 3.6: Photolumunescence of 1mg of micro-pSi functionalized with heptene suspended in 2ml toluene.

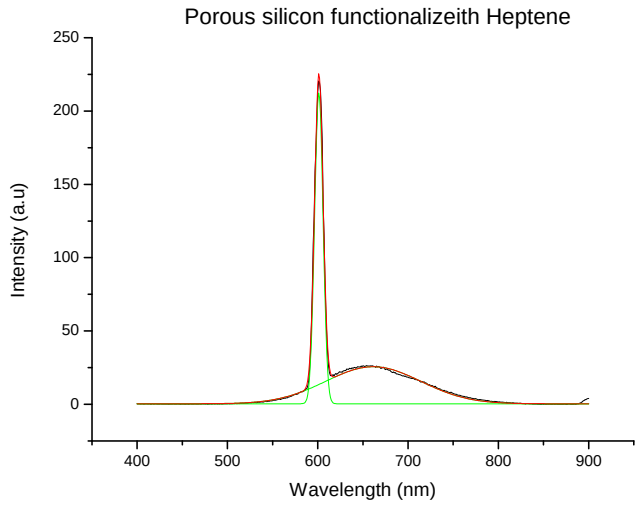

Figure 3.7: Photolumunescence of 1mg of micro p-Si functionalized with heptene suspended in 2ml toluene.In this case there is only one red band. In figure we reported in green the gaussian deconvolution curves, in red the fitting one and in black the data collected.

At difference from the naked porous silicon this functionalized particles present only one red band shown in Figure 3.7. Repeating the same gaussian deconvolution procedure we found that the starting luminescence is $\lambda = 662 \pm 5nm$ this is in good agreement with the visible color of the sample reported in Figure3.6.

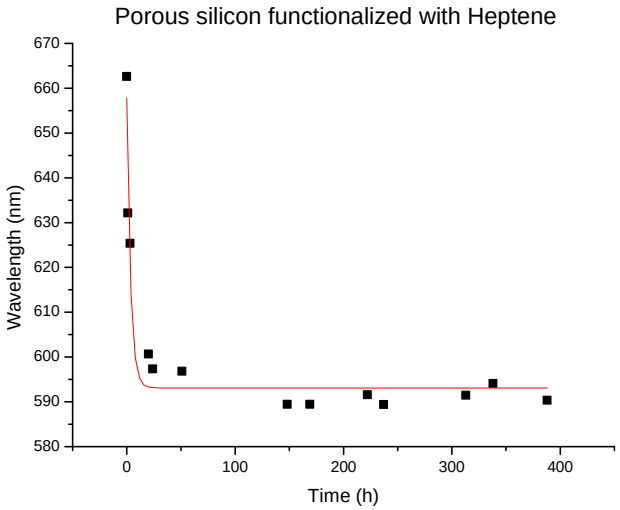

Figure 3.8: Time dependance emission wavelength of 1mg of micro-pSi functionalized with heptene suspended in 2ml toluene. The red curve is the exponential fit. The errorbars are inside the dots.

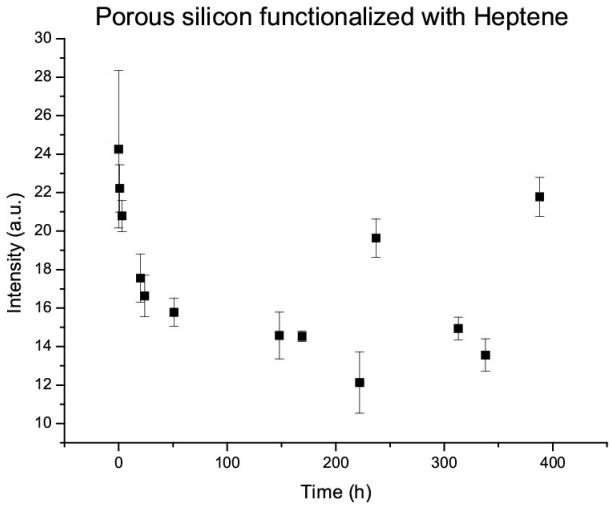

Figure 3.9: Time dependance of the PL intensity of 1mg of micro p-Si functionalized with heptene suspended in 2ml toluene. We can't define any kind of trend.

We observed time dependence for the wavelength emission and intensity of the microparticles functionalized with heptene is similar to that of the naked ones. The only remarkable difference was the lack of a defined trend of the intensity decay after 200 hours. This is probably due to the aggregation of the hydrophobic particles. The aggregates are partially dissolved by shaking the sample before each experimental measurements. Using the same fit procedure described above we find that: the wavelengths of the peak emission seem to stabilize at approximately $\lambda = (593 \pm 5)nm$ and the time constant resulted to be:$\tau = (4 \pm 1)hours$.

Porous silicon after HF attack

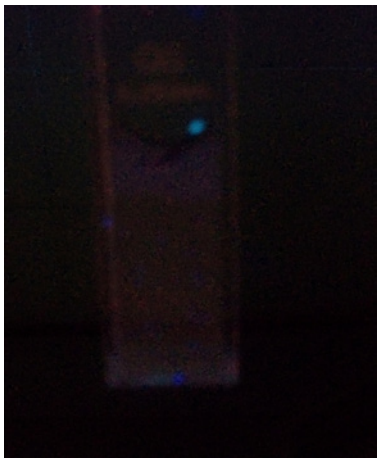

Figure 3.10: Photoluminescence of 1mg micro-pSi after acid attack suspended in 2ml toluene.

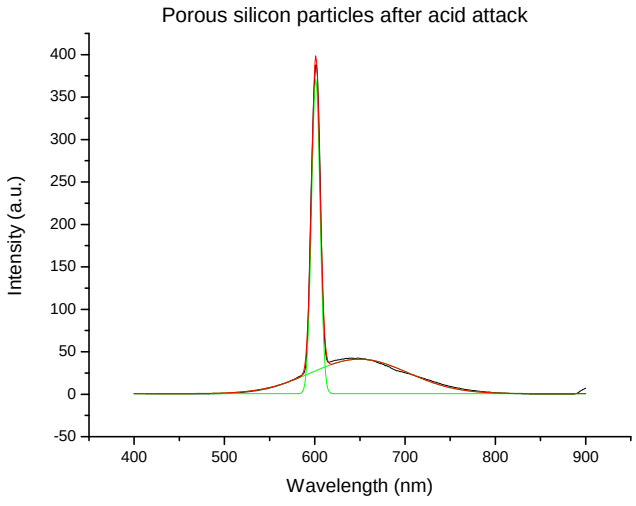

Figure 3.11: Photolumunescence of 1mg of microp-Si after acid attack suspended in 2ml toluene.Again in this case there is only one red band. In figure we reported in green the gaussian deconvolution curves, in red the fitting one and in black the data collected.

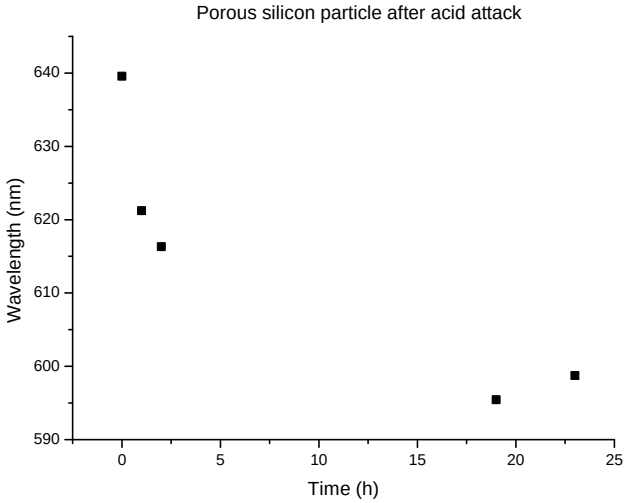

Figure 3.12: Time dependance emission wavelength of 1mg of micro-pSi after acid attack suspended in 2ml toluene. The red curve is the exponential fit. The errorbars are inside the dots.

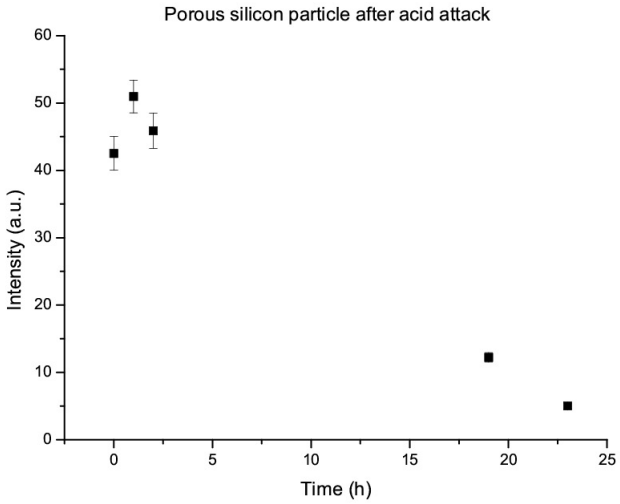

Figure 3.13: Time dependance of the PL of 1mg micro p-Si after acid attack suspended in 2ml toluene.

In this case the luminescence lasted less then 24 hours, therefore we can not make any estimation.

Porous silicon after the last functionalization

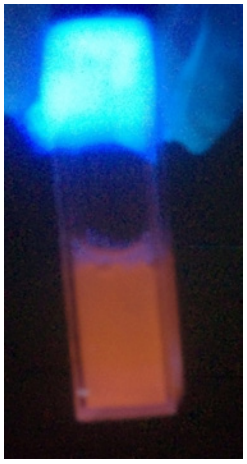

Figure 3.14: Photoluminescence of 1mg micro p-Si after the second functionalization with acrylic acid suspended in 2ml toluene.

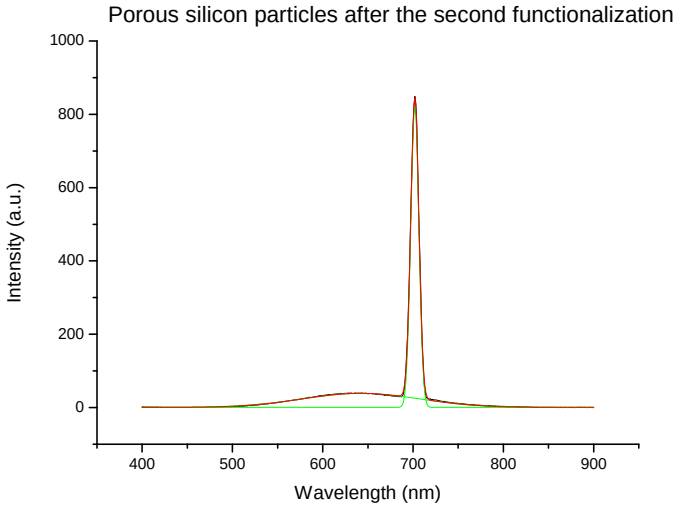

Figure 3.15: Photoluminescence of 1mg micro p-Si after the second functionalization with acrylic acid suspended in 2ml toluene.Again in this case there is only one red band. In figure we reported in green the gaussian deconvolution curves, in red the fitting one and in black the data collected.

We can appreciate the reappearance of the red band, as pictured in Figure 3.15. Repeating the same gaussian deconvolution procedure we found that the starting luminescence is $\lambda = 642 \pm 5nm$.

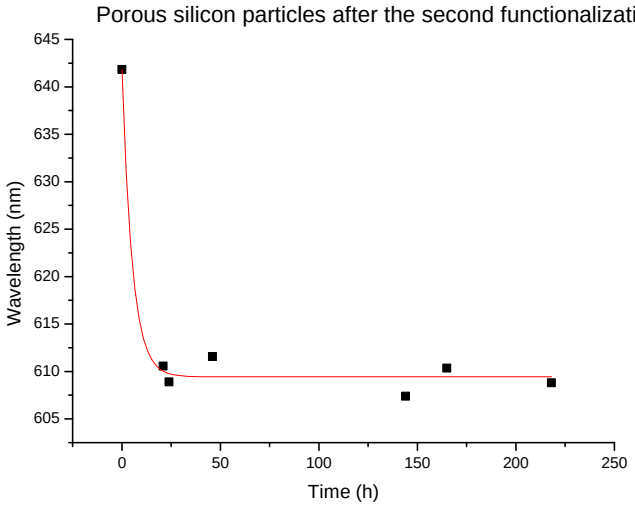

Figure 3.16: Time dependance emission wavelength of 1mg of micro-pSi after the second functionalization with acrylic acid suspended in 2ml toluene. The red curve is the exponential fit. The errorbars are inside the dots.

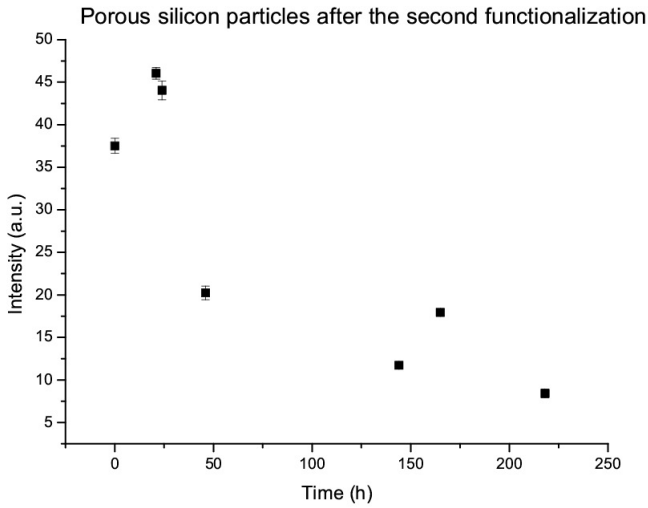

Figure 3.17: Time dependance of the PL of 1mg micro-pSi after the second functionalization with acrylic acid suspended in 2ml toluene.

As visible in Figure 3.16 we found that, after the second functionalization, the wavelengths of the peak emission seem to quickly approach a stability at approximately $\lambda = (609 \pm 5)nm$ and remain stable for around 10 days, after this interval the luminescence dropped and we became unable to detect it. Even if short, the lifetime of this material, is enough to calculate its time constant $\tau = (5 \pm 3)hours$ from the fit presented in Figure 3.16.

3.0.7 FTIR spectra

The aim of FTIT measurements was to identify and to characterize the main peaks of the FTIR spectra linked to the different stages of surface modification procedure. In order to provide a chemical characterization of the material.
As previously said, at the beginning of the "Experimental Section", FTIR analysis provides a quantitative result that is not spatially resolved, since it collects information from a sample depth range up to 700-850 nm and so it can't distinguish between inner and outer surfaces of the pores.

For this type of characterization we were forced to use only the Luminescent preparation since the Non Luminescent one presented a interference profile that made the analysis impossible.

Data collection
All Fourier Transform Infrared (FTIR) spectra were acquired using a micro-FTIR Nicolet iN10 instrument equipped with a liquid nitrogen cooled detector (Figure 3.18).

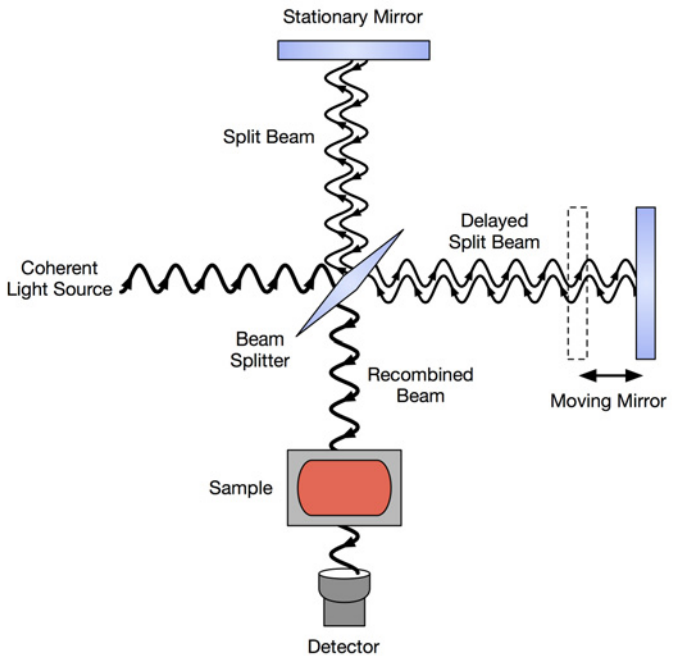

Figure 3.18: Microftir working scheme.

Starting from a freshly etched sample we monitored the impact of the surfaces modification throughout the whole procedure, deposing a small amount of dried silicon powder on a zinc selenide support after each step of the functionalization.
To minimize the oxidation reactions of the naked porous silicon surface, which are very fast, the samples were stored under dry nitrogen atmosphere until the measurement.

Data analysis

we localized 5 different areas containing a sufficient amount of p-Si. Each probed area was 50x50, to include several microparticles In order to have a better statistic for each sample we acquired 5 spectra probing 5 different areas containing a sufficient amount of p-Si to cover the entire area of acquisition.

All spectra were acquired using the same setup conditions:

- probed sample area was chosen to be $50\mu m \times 50\mu m$, in order to include a sufficient number of p-Si microparticles to cover the entire area of acquisition.
- for each final spectrum the instrument automatically collected and mediated 256 spectra in order to minimize the background effect.
- scanned range was 750-4000 $cm^{-}1$ with a 4 $cm^{-}1$ resolution.
- The background spectrum was collected before each set of measurements, using a total reflecting gold plate as reference sample. The background spectrum was subtracted from the p-Si spectra.

We estimated the wavelength number and the intensity of the peaks by fitting them with a convolution of lorentzian curves (an example is reported in Fig.3.21); we then mediated on each set of 5 acquisition in order to obtain a better statistic and the errors were calculated as standard deviation or propagation depending on the cases.
We noticed that (as clearly visible in the example Fig.3.19) some spurious signals were present and the baseline was not straight in spite of the baseline subtraction. This instability was probably due to the the detector heating and to changes in local air composition. The irregular baseline is due to the sample irregular shape and to the presence of broad silicon oxide peaks. For this reasons we proceed to apply an *a posteriori* correction of the ground to each individual spectrum(example Fig.3.20) by fitting the baseline.

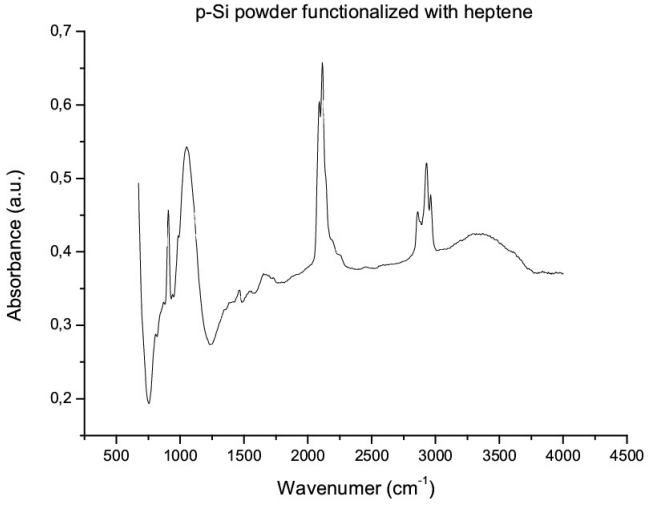

Figure 3.19: Examples of p-Si FTIR spectra.

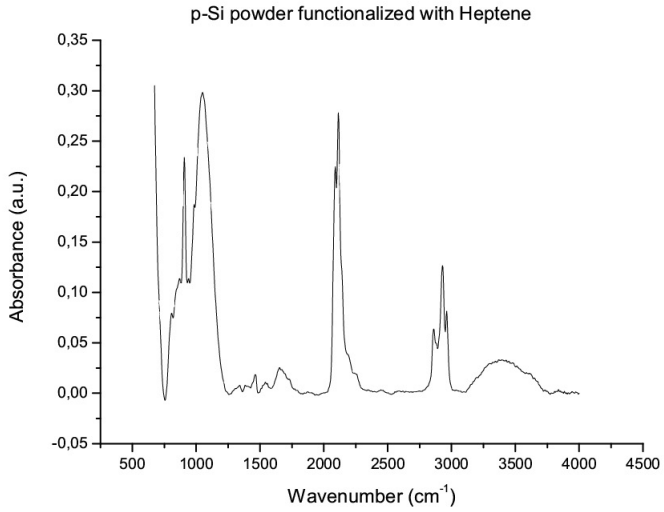

Figure 3.20: Examples of p-Si FTIR spectra after the ground correction.

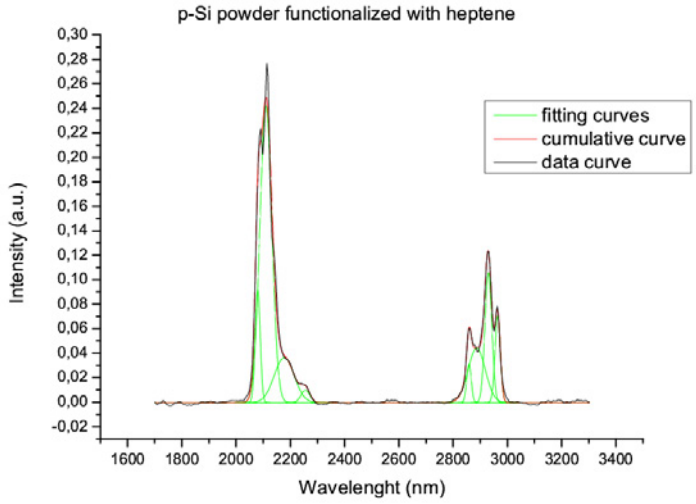

Figure 3.21: Examples of fitted p-Si FTIR spectra after the ground correction.

In Figure 3.19 we can see the typical feature of p-Si and of the organic molecules grafted on it. In particular we can appreciate the presence of the following peaks:[38]

wavenumber (cm^{-1})	bond	type of vibration[38]
925	$Si-H_2$	bending
1100	$Si-O$	stretching
2110	$Si-H$	stretching
2860	$C-H_2$	stretching
2938	$C-H_3$	stretching
2955	$C-H_3$	stretching
3400	$Si-OH$	stretching

Our aim was to provide a significant characterization for each step of our procedure in order to be able to detect eventual variation in the surface composition.
For this reason we focused our attention on the the peaks which can be considered as significant probe of the surface chemical composition: [38][39]

- $Si-H$ bond (peak around 2100 cm^-1), that are used as the grafting point of both, heptene (or 11-br undecene) and acrylic acid. These kind of bonds are present on freshly etched material and are again exposed after the acid attack which removes the organic layer. The surface density of these groups is expected to be higher on freshly etched pSi and after the exposure to HF.
- $Si-CH_x$ bond (peak around 2800-3000 cm^-1), these are characteristic of alkyl chains and so, they appear after the functionalization with heptene (or br undecene) and with acrylic acid. These groups are removed by the HF treatment.
- $C=O$ bond (peak around 1720 cm^-1), this belongs to the carboxylic group ($Si-COOH$) introduced by the functionalization with acrylic acid.

For this reason we restricted our analysis to the spectral interval between $1700cm^{-1}$ and $3300cm^{-1}$ searching for the first two groups and between $1450cm^{-1}$ and $3350cm^{-1}$ if we were looking for all three of them, depending on the cases.

In consideration of the fact that spectra taken on different samples are not directly comparable, we decided to consider the ratio between $Si-CH_x$ or $Si-COOH$ and $Si-H$ absorbance intensity as a quantitative parameter which lets us to compare different samples and treatment.
Since this parameter provides the estimation of the surface density of the functional organic groups (CH_x and COOH) with respect to the free grafting centers of silicon, that is the SiH groups, we decided to call it index of coverage(IC).

I set of measurements

This set of measurements was performed to test our capability to properly functionalize the surface of the porous silicon particles and in particular we were interested in proving the efficiency of the masked acidified procedure in removing the alkylic chains and replacing them with $Si-H$ bonds. Also we wanted to prove that this bond was then made available for a further functionalization and that it was possible to graft the reactive Si-H species to carboxylic groups via stable Si-C bonds.
Figure 3.22 I reports the spectra of p-Si microparticles acquired after each step of functionalization.

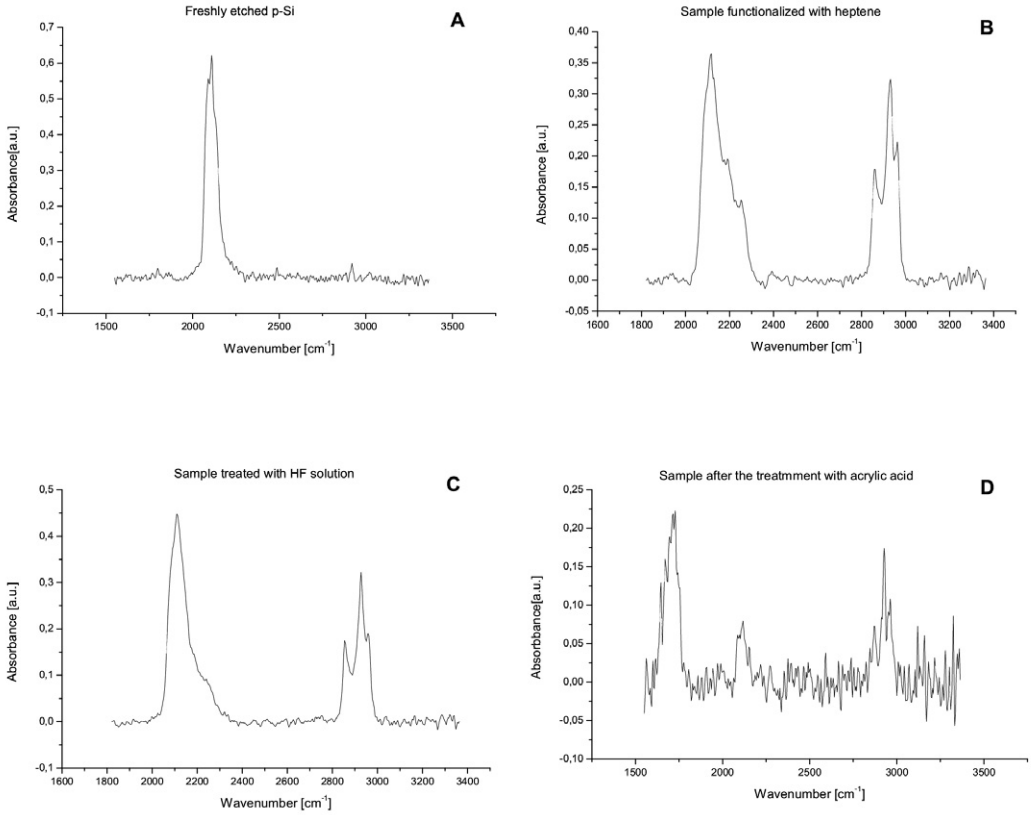

Figure 3.22: FTIR spectra of p-Si powder. A)freshly etched; B)hydrosilylated with heptene; C) after the acid attack; D)after the second hydrosilylation with acrylic acid.

As we expected, the freshly etched material presents just the peaks of the $Si-H$ bond at $2100-2300cm^{-1}$(Figure3.22A).
After the thermal hydrosilylation with heptene(Figure 3.22B) it is clearly visible the appearance of four peaks inbetween $2800cm^{-1}$ and $3000cm^{-1}$ associated with the $C-H_x$ stretch vibrations of the alkylic chains.
In Figure 3.22C we can see that the intensity of the $Si-H$ peaks increases while the $C-H_x$ ones proportionally decrease. This is what we expected after the acid attack which should generate a hydrogen terminated outer layer by removing the alkylic chains from the outer surface.
Finally in Figure 3.22D is possible to appreciate the appearance of a new peak at around $1700cm^{-1}$ corresponding to the carboxylic group consistent with what we expected after

the functionalization with acrylic acid.

The assignations of the peak relevant for this work are given in table 3.1. As it is clearly visible in Figure 3.22D the last spectra was really noisy due to the fact that the detector was not cooled enough when the measurements were done, this made hard to identify the peaks and to obtain a semi quantitative analysis. For this reason we decided, just for this spectra, to identify the peaks as local maximum rather the to fit them.
The noisy background is also the cause of the missing identification of two peaks.

Wavenumber $[cm^{-1}]$				Type of bond
A	B	C	D	
			1713 ± 6	$\nu C = O$
2112,11	2106± 4	2105±2	2098 ± 8	$\nu Si - H$
	2183± 5	2167±13	2143± 7	$\nu Si - H$
	2260± 5	2247±12		$\nu Si - H$
	2860± 6	2859±4	2867 ± 14	$\nu C - H_2$
	2899± 12	2908±14		$\nu C - H_2$
	2937± 4	2934±4	2929 ± 5	$\nu C - H_3$
	2945± 4	2944±4	2965 ± 6	$\nu C - H_3$

Table 3.1: Most relevant peaks assignations of p-Si powder. A)freshly etched; B)hydrosilylated with heptene; C) after the acid attack; D)after the second hydrosilylation with acrylic acid.

All values are compatible with the ones found in literature [32][40][38].
A more detailed overview on the chemical modification of the particle surfaces can be obtained analyzing the index of coverage, we recall that the higher this ratio the more Si-H groups should be available for further functionalization.

Peak$[cm^-1]$	Index of coverage			Variation(%)	
	B	C	D	C/B	D/B
1700 $\nu C = O$			3± 1		
2100 $\nu Si - H$	1	1	1		
2856 $\nu C - H_2$	0,3± 0,13	0,23± 0,05	0,9± 0,4	73	290
2878 $\nu C - H_2$	0,5± 0,05	0,32± 0,07		71	
2922 $\nu C - H_3$	0,7± 0,14	0,52± 0,13	1,2± 0,5	72	164
2960 $\nu C - H_3$	0,5± 0,12	0,35± 0,08	1,1± 0,5	70	226

Table 3.2: Index of coverage p-Si powder. B)hydrosilylated with heptene; C) after the acid attack; D)after the second hydrosilylation with acrylic acid.

We can see in table 3.2 that the etching with HF of the p-Si functionalized with heptene, determines a decrease in the index of coverage of 29% corresponding to a growth of the ratio between Si-H and alkylic chains of 41%.
The standard deviations of these measurements are large, as expected for samples made of p-Si microparticles, which undergo a modification reaction involving just the external surface. However the average values of the IC indicates quite clearly that some alkyl chains are replaced by free SiH groups.
This implies that the acid has efficiently attacked the surface and removed part of the alkylic chains letting the surface bearing Si-H functionalities.

Looking at $1720 cm^{-1}$ ascribed to the C=O of the carboxylic group we can notice that the index is greatly increased in respect both to the sample treated with heptene and to that trated with 1%HF. This suggests that the thermal hydrosilylation with acrylic acid acts not only on the external sites, but also on the inner ones left uncovered during the first functionalization.

II sets of measurements

With this experiment we aimed to test the effect of different concentration of hydrofluoric acid solution on the amount of alkylic chains removed and thus of sites made free for new functionalization.

For this purpose all samples were prepared from the same starting p-Si powder, functionalized with heptene, that was then treated with aqueous solutions containing different concentrations of hydrofluoric acid. In particular we tested aqueous solutions containing 0.1%, 1% and 2% HF.

In Figure 3.23 we report the spectra of the pSi after the treatment with the various HF solutions.

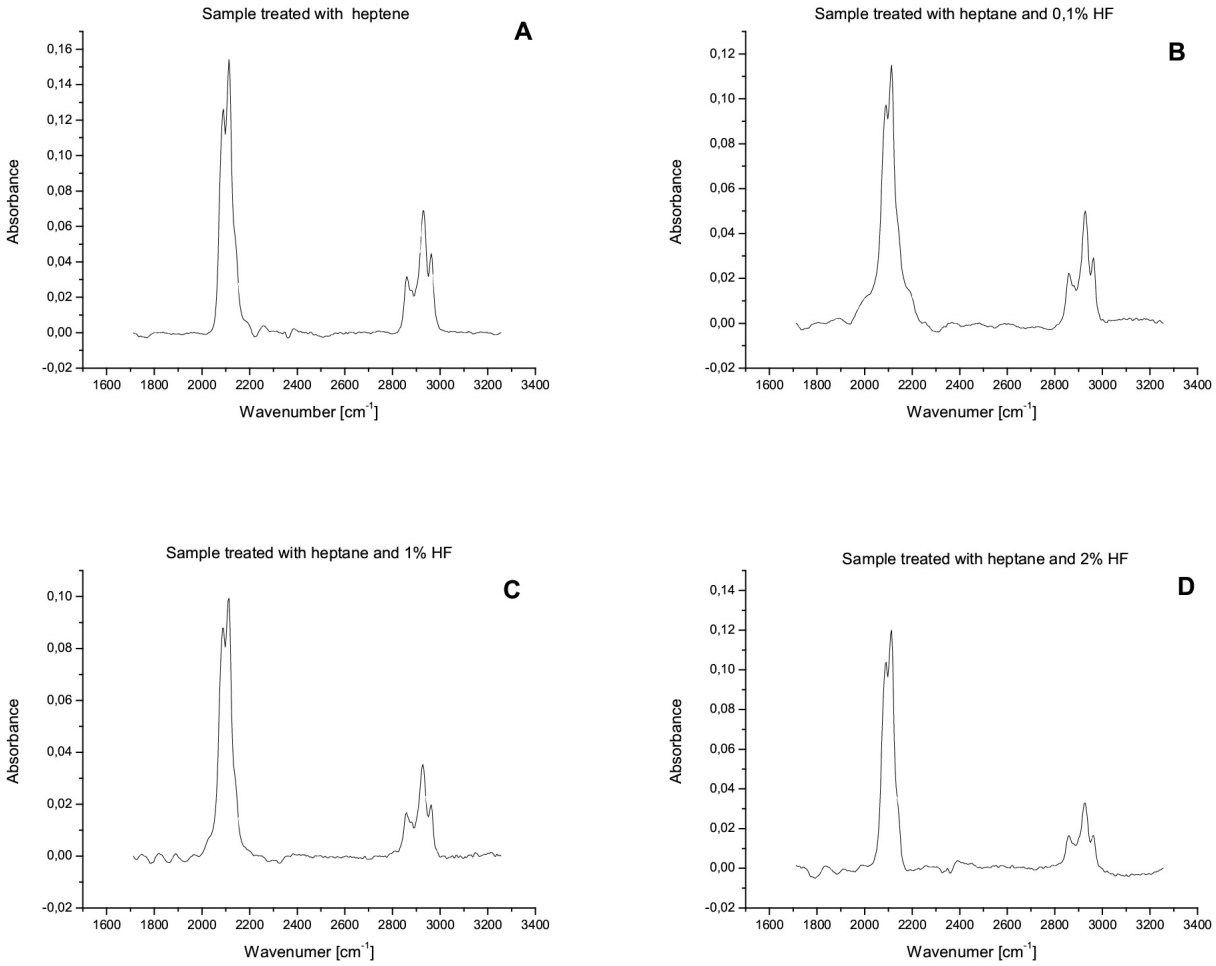

Figure 3.23: FTIR spectra of p-Si powder. A)freshly etched; B)hydrosilylated with heptene; C) after the acid attack; D)after the second hydrosilylation with acrylic acid.

In Table3.3 are shown the wavenumbers of the characteristic peaks and in Table 3.4 we listed the IC for the different samples.

Wavenumber $[cm^{-1}]$				Type of bond
A	B	C	D	
2079± 10	2092± 9	2080± 11	2086± 7	$\nu Si-H$
2108± 7	2103± 5	2107± 6	2111± 7	$\nu Si-H$
2858± 4	2857± 4	2860± 4	2858± 5	$\nu C-H_2$
2892± 15	2903± 12	2891± 8	2885± 7	$\nu C-H_2$
2930± 4	2921± 4	2928± 4	2927± 4	$\nu C-H_3$
2964± 4	2963± 4	2964± 6	2963± 4	$\nu C-H_3$

Table 3.3: Assignations of the most relevant peaks of p-Si powder. A)freshly etched; B)hydrosilylated with heptene; C) after the acid attack; D)after the second hydrosilylation with acrylic acid.

As for the previous case the wavenumbers of the peak assignations are in accord with the literature, [32][40][38].

Peak[cm^-1]	Index of coverage			
	A	B	C	D
2856 $\nu C-H_2$	0,15 ±0,07	0,16 ±0,03	0,13 ±0,07	0,10 ±0,03
2878 $\nu C-H_2$	0,18 ±0,08	0,17 ±0,02	0,15 ±0,08	0,12 ±0,04
2922 $\nu C-H_3$	0,45 ±0,21	0,39 ±0,10	0,32 ±0,17	0,31 ±0,07
2960 $\nu C-H_3$	0,295±0,12	0,25 ±0,04	0,21 ±0,12	0,20 ±0,06
	B/A(%)	C/A (%)	D/A(%)	
	103	90	71	
	91	73	69	
	88	72	70	
	86	74	68	

Table 3.4: Index of coverage p-Si powder functionalized with heptene and treated with:A)nothing else, B) 0.1% HF solution, C) 1% HF solution, D) 2% HF solution.

The data shown in Table 3.4 indicates that the efficiency of the removal of alkyl chains depends on HF concentration. Analyzing the second part of Table3.4 it is made clear that the 0.1% HF solution treatment, causing a decrease in the index of coverage of just 12%, is not strong enough to remove properly the alkylic bonds from the outer surface. At difference from using 1% and 2% HF solution we obtain a decrease in the index of coverage of 27% and 30% respectively leading to a growth of the ratio between Si-H and alkylic chains of 38% and 45%.

We have noticed that on p-Si layer the treatment with 2% HF solution produce an uneven functionalization and surface, conversely of the 1% solution treated ones. The uniformity of the surface after 1% HF treatment was also confirmed by the contact angle as reported in the following chapter. For these reasons we believe that 1% Hf solution is the most suitable choice for our purpose.

3.0.8 Contact angle

This type of characterization was performed in order to produce a qualitative information about the hydrophilicity/hydrophobicity of the surface by studying the variation of the contact angle of a water drop deposited on silicon porous layer after each step of the functionalization.

Data collection

The contact angle was characterized using the home-made apparatus showed in Figure 3.24. For this kind of analysis we used the porous silicon layer still attached to the wafer. We positioned the specimen onto a support and then a drop of deionized water of known volume ($2\mu l$) was deposited ontop of it by using a microsyringe. Right after the deposition we were able to collect 5 images focused on the drop thanks to a USB camera coupled to an optical zoom positioned over a movable support and with a spatial resolution of about $10\mu m$. In correspondence we acquired also a picture focused on the frontal section of the silicon suitable as background for the further analysis.

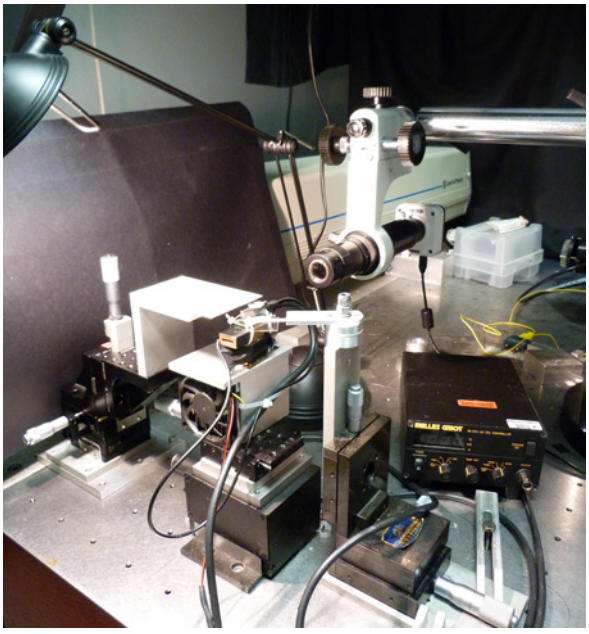

Figure 3.24: Picture of the set up used to measure the contact angle.

Data analysis

For each sample we deposited and analysed, with the same technique, three different drops of water in order to obtain a mean information about the chemistry of the surface and to avoid a misrepresentation.

All the samples were kept in a nitrogen saturated environment till the moment of the analysis that generally occurred the day after the preparation. The images were collected with the software: Motic Images plus 2.0 while the analysis was performed using ImageJ.

As for the previous section we will report the data obtained by the different p-Si preparations, since this type of analysis is highly influenced non only by the chemistry of the surface but also from the porosity of it.

Luminescent porous silicon

In this section we here reported the analysis of the hydrofilicity/hydrophobicity of the porous silicon at different stages of the preparation. Is important to stress that all the samples analyzed below came from a single wafer functionalization procedure. In particular our samples were obtained removing part of the main sample after each step of the procedure in order to obtain a consistent set of data.

In Figure 3.25 are reported the characteristic images of contact angle of a liquid droplet deposited on a rigid solid surface for luminescent porous silicon.

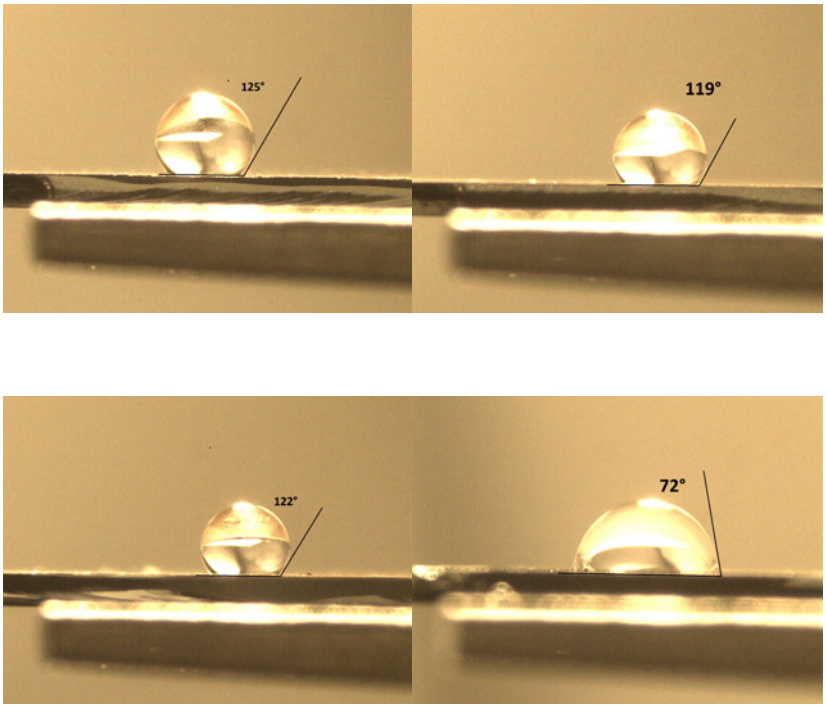

Figure 3.25: Contact angle of a liquid droplet deposited on a porous silicon layer: A)freshly etched; B)hydrosilylated with heptene; C) after the acid attack(HF1%); D)after the second hydrosilylation with acrylic acid

In table 3.5 are given the contact angles for the different stages of the functionalization, in particular we identify :

- A freshly etched silicon layer;
- B sample hydrosilylated with heptene;
- C sample after the acid attack (HF1%);
- D sample after the second hydrosilylation with acrylic acid;

the errors reported are calculated as standard deviation.

Luminescent porous silicon			
Sample type	Angle sx	Angle dx	Mean Angle
Naked (A)	125 ± 1	124 ± 1	125 ± 1
Heptene (B)	120 ± 2	118 ± 1	119 ± 2
HF 1% (C)	124 ± 1	121 ± 1	123 ± 2
Acrylic acid (D)	72 ± 2	71 ± 2	72 ± 2

Table 3.5: Contact angle of a liquid droplet wetted to a p-Si surface

From table 5 we can observe that the right and left angles are equal within the error for all four samples, therefore we can safely suppose that the surface was functionalized evenly.

We can also underline that as we expected the naked material, bearing $Si - H$ bonds, is hydrophobic and it becomes only slightly more hydrophilic after the hydrosilylation with heptene since in this case the surface display CH_2 and CH_3 bonds.[8]

With the acid attack the majority of the alkylic chains present on the outer surface were removed and the Si-H groups were restored; for this reason the contact angle rises again and reach almost the value of the naked material. This lead us to believe that the change in the contact angle is almost entirely due to the surface chemical modification and not to a possible variation of the porous structure of the material.

After the functionalization with the acrylic acid the surfaces becomes more hydrophilic confirming that the COOH groups have been introduced. The sample present a contact angle reduced by about 42% lower than the one treated with hydrofloridric acid. This suggest, along with the symmetry of the drops, that at the end of the procedure the surface was successfully functionalized with the acrylic acid.

However this kind of experiment can give just a qualitative idea of the surface chemistry, but can't produce any kind of evidence about the internal structure or about the level of functionalization. The measurement of the contact angle confirm that the chemical composition of the external surface is in line with the kind of modification procedure we applied. The limit of this approach is that the information we obtained concern the external surface and we do not know what happened inside the pores.

Non luminescent porous silicon

This set of measurements was performed to test the effect of the acid attack related to the HF concentrations.

For this reason we prepared 4 samples treated with two different concentration of HF plus 2 of control.
The silicon wafer was etched and then hydrosilylated using heptene(specimen type A).The pSi sample so obtained was devided in three parts: two of which were treated with hydrofluoric acid respectively at 0.1% and 1%(specimen type B and C). The three samples so obtained were divided into two parts by cutting them with a diamond bit.
For each kind of sample one half was set aside while the other half was functionalized with acrylic acid(specimen type D, E and F).
At the end we obtained the following 6 samples:

A. sample hydrosilylated with heptene;

B. sample hydrosilylated with heptene and attacked with hyfrofloridric acid at 0.1% ;

C. sample hydrosilylated with heptene and attacked with hyfrofloridric acid at 1% ;

D. sample A hydrosilylated with acrylic acid;

E. sample B treated with 0.1% HF and then hydrosilylated with acrylic acid;

F. sample C treated with 1% HF and then hydrosilylated with acrylic acid.

Again in Figure 3.26 are reported the characteristic images of contact angle of a water drop on a Non Luminescent porous silicon layer.

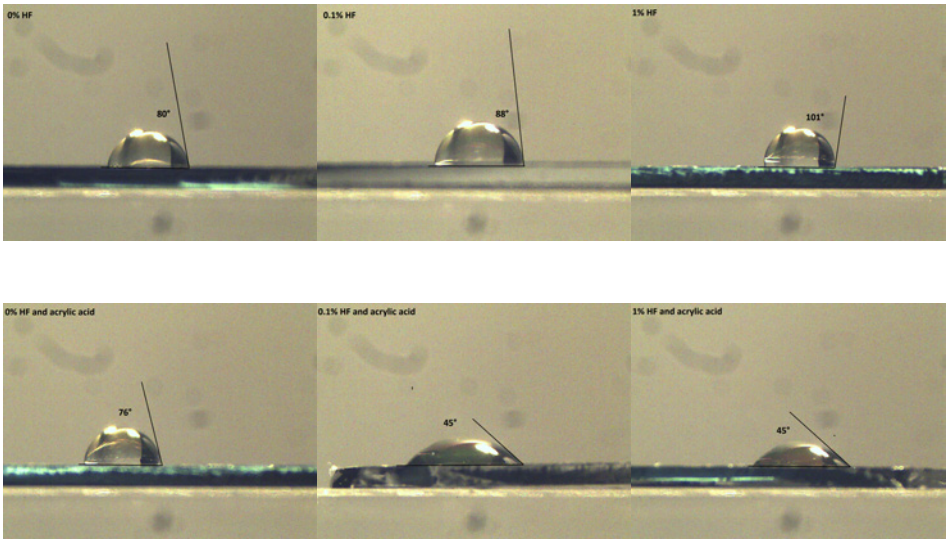

Figure 3.26: Contact angle of a liquid droplet deposited on a porous layer of Non Luminescent porous silicon type : A sample hydrosilylated with heptene; B sample hydrosilylated with heptene and attacked with hydrofluoric acid at 0.1% ; C sample hydrosilylated with heptene and attacked with hydrofluoric acid at 1% ; D sample A hydrosilylated with acrylic acid; E sample B treated with 0.1% HF and then hydrosilylated with acrylic acid; F sample C treated with 1% HF and then hydrosilylated with acrylic acid.

In table 3.6 are given the contact angle values for the different preparations, the errors reported are calculated as for the previous case as standard deviation.

Non Luminescent porous silicon			
Sample type	Angle sx	Angle dx	Mean Angle
Heptene (A)	80 ±1	80 ± 1	80 ± 1
HF 0.1% (B)	88 ±1	88 ± 1	88 ± 1
HF 1% (C)	101 ±1	101 ± 1	101 ± 1
sample A + acrylic acid(D)	77 ±1	75 ± 1	76 ± 1
sample B + acrylic acid(E)	45 ±1	46 ± 1	45 ± 1
sample C + acrylic acid(F)	45 ±1	45 ± 1	45 ± 1

Table 3.6: Contact angle assignation

As for the previous scenario the right and left angles match within the errors so we can safely say that the drop are symmetrical and that the surface is uniform.

First of all we can notice that for the specimen (A and D) which did not undergo the treatment with HF, the angle present a decrease of 4%. This variation is compatible with the fact that with our first hydrosilylation(as seen with the FTIR analysis) we weren't able to saturate all the Si-H bonds so some of them were left available for a further functionalization, leading to a decrease of the contact angle.

As for the Luminescent porous silicon case, after the treatment with the Hydrofloridric acid and the hydrosilylation with acrylic acid the contact angle drastically drops to around half of the starting value.
This data confirm that after the first hydrosilylation with heptene the surface was properly functionalized and that the acid attack truly removes the $-CH_2$ and $-CH_3$ groups in order to replace them with the $-COOH$ after the second hydrosilylation.

We also want to stress that the value of the angle after the acrylic functionalization for sample E and F match within the error. This datum suggests that even at low HF concentration (0.1%) the removal of the surface silicon layer has occurred.

This guarantees us the possibility to choose the Hf concentration of the acid attack step on the base of the functionalization of the inner surface examined with the other types of analysis, since it doesn't affect the external surface functionalization.

Thus it is compatible with the choice we made, after the FTIR analysis, of using an HF concentration of 1%.

Since XPS and Raman spectroscopy involved the usage of samples prepared using 11-bromo-1-undecene wechecked if the pSi functionalized by this compound shows a surface wettability similar to that functionalized with heptene.
Our aim was to prove that even if we used a alkylic chain this doesn't really affect the final outcome.
To prepared the samples we used the same procedure as before with the difference that

in this case we used 11-bromo-1-undecene in the first functionalization step. In the specific case we first produced the porous silicon layer(specimen A) from the Non Luminescent porous silicon silicon type then proceeded with the hydrosilylation with 11-bromo-1-undecene (specimen B). The sample was then divided into two parts, one of which was acidified with a waterbased HF solution at 1% (specimen C). At this point both part were cut again in half and one part of each specimen was functionalized with acrylic acid (specimens D and E obtained respectively from specimens C and D).

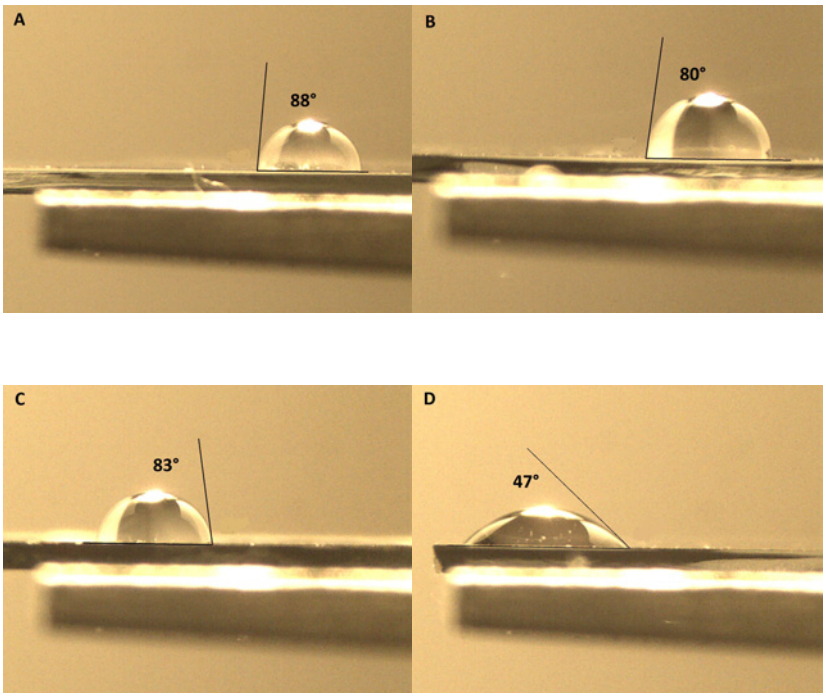

Figure 3.27: Contact angle of a liquid droplet deposited on a rigid solid surface for : A)hydrosilylated with 11-bromo-1-undecene; B) after the acid attack; C)after the second hydrosilylation with acrylic acid but without the HF treatment D)after the second hydrosilylation with acrylic acid .

Non Luminescent porous silicon			
Sample tye	Angle sx	Angle dx	Mean Angle
B	88 ±1	88 ± 1	88 ± 1
C	80 ±1	80 ± 1	80 ± 1
D	83 ±1	83 ± 1	83 ± 1
E	47 ±1	47 ± 1	47 ± 1

Table 3.7: Most relevant peaks assignations.

Again for this sample the drops are all symmetric as observed in all the other measurements and all we have said in the previous analysis still apply.
In particular we found that this result are similar to the ones obtained in the case of Non Luminescent porous silicon layer functionalized with heptene, suggesting that the use of

a different alkene does not affect significantly the sample characteristics.
For this reason we can safely proceed with the XPS and Raman analysis supposing that the, as obtained, results can be applied also to the Non Luminescent porous silicon treated with heptene.

3.0.9 X-ray photoelectron spectroscopy (XPS)

In this chapter we are going to discuss the results of the XPS characterization; this measures the elemental composition of the Si layer surface and produces a quantitative spectroscopic result.
The XPS spectra were acquired at different tilting angles to obtain the surface composition profile along the p-Si pores, providing us a more specific information about spatial distribution of the chemicals both within and on the surface of the pores.

Data collection
XPS spectra of micro-pSi particles were acquired thanks to a collaboration with Dr.Nadhira Bensaada Laidani of the FBF(Bruno Kessler Foundation) who provided also the anlysis of the spectra.
All data were acquired using Scienta ESCA 200. For this kind of analysis we used the non luminescent type of preparation, since this measure is highly sensible to photoelectrons. The samples were prepared and cut into squares of $1cm \times 1cm$.

Data analysis
The basic mechanism of surface sensitivity enhancement at grazing emission angle [41] is illustrated in Fig.3.29.

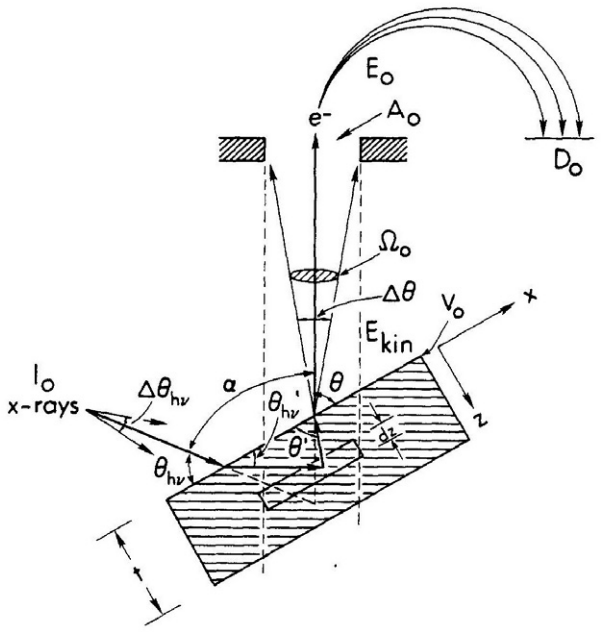

Figure 3.28: Idealized spectrometer geometry for calculating angular-dependent photoelectron peak intensities, various important parameters and variable indicated. In particular: $\alpha = 45°$ is the angle between the incident X-ray beam ($\theta_{h\nu}$) and the photoemission angle, Ω_0 is the effective solid angle acting over an effective source area of A_0, D_0 is the detection efficiency.[41]

Known [41] that the relationship that links the tilting angle to the intensity contribution from a depth z is, in first approximation:

$$I_k(z) = I_k(z=0)C_K(\Lambda_e(E_K), \theta, z) \tag{3.1}$$

with:

$$I_k(z=0) = I_0\Omega_0(E_K)A_0(E_K)D_0(E_K)\rho_K(d\sigma_K/d\Omega)\Lambda_e(E_K) \tag{3.2}$$

$$C_K(\Lambda_e(E_K), \theta, z) \propto \gamma exp(-z/\lambda cos\theta) \tag{3.3}$$

where: θ is the angle between the surface normal and the analyzer direction("photoemission angle"), and Λ_e the inelastic mean free path of the photoelectrons.
I_0 is the intensity of the incident uniform flux of X-rays, Ω_0 is the effective solid angle acting over an effective source area of A_0. D_0 is the detection efficiency and $d\sigma_K/d\Omega$ is the cross section while ρ_K is the density of the atoms ore molecules on which subshell k is located.
C_K is a morphological parameter of correction and contains also the dependance from the angle θ and γ is the fraction of surface area covered by the overlayer.[41]

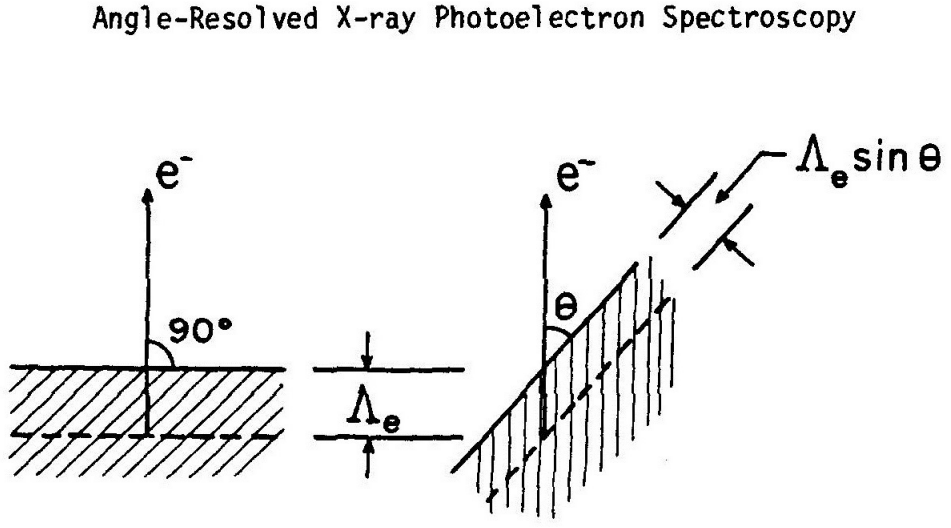

Figure 3.29: Illustration of the basic mechanism producing surface sensitivity enhancement for low electron exit angle θ. The average depth for no-loss emission as measured perpendicular to the surface is $\Lambda_e sin\theta$, being Λ_e the mean free path for inelastic scattering.

As shown in Fig.3.29 the depth of the analysis is determined by the attenuation function of the emitted electrons, $\Lambda_e exp(-z/\lambda cos\theta)$. In silicon Λ_e corresponding to an incident electron with energy $E_{h\nu} = 1486.7eV$ is around 3nm; this means that from the point of view of this analysis our samples are seen as rough and not porous, since the depth of

penetration doesn't allow us to distinguish the pore structure.[42][43]
Moreover since the peaks intensity also depends on the attenuation function (eq.3.1-3.3), it is possible to use the variation in depth analysis to produce a depth profile of the detected signals.

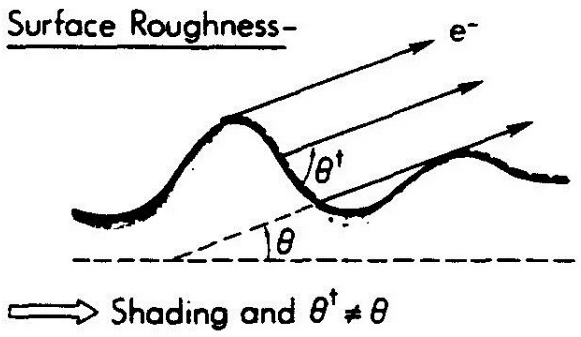

Figure 3.30: Illustration of surface roughness effect.

The qualitative effects of surface roughness is that certain regions on the surface may be shaded for emission at a given θ by adjacent raised areas, as indicated by the cross-hatched region. Such shading will tend to be negligible if the roughness are small with respect to typical Λ_e, as for our case. The precise form of the actual effect depend strongly on the exact configuration of the profile, although in the limit of small roughness and of rounded contours, as ours, the XPS analysis produces reasonable result.[41][42][43] Thus roughness must be kept in mind as possible source of deviation however it doesn't preclude the possibility to obtain a semi-quantitative depth profiling.
XPS analysis can provide only a semi-quantitative result since, due to the sample morphology, it is impossible to properly evaluate the roughness factor C_K (eq.3.3)for our surface without a complementary examination.
Besides, it is important to underline that at $\theta = 50°$ the X-ray beam impinges normally to the porous silicon surface and so it is aligned with the pore direction of growth, causing a deviation from the real value.

After the data collection the ground was subtracted using the Shirley method [44] and the as obtained spectra were fitted in order to determinate the energy of the maximum of the main peaks and their full width half maximum. These are the two parameters that allowed us to identify the elements and their oxidation state.
Semi quantitative information are obtained through the values of the peaks area corrected by the cross section relative to the specific photoelectronic process. If there was a superposition of the peaks a deconvolution was used.
In Figure 3.31 is shown an example of fitted p-Si XPS spectra.

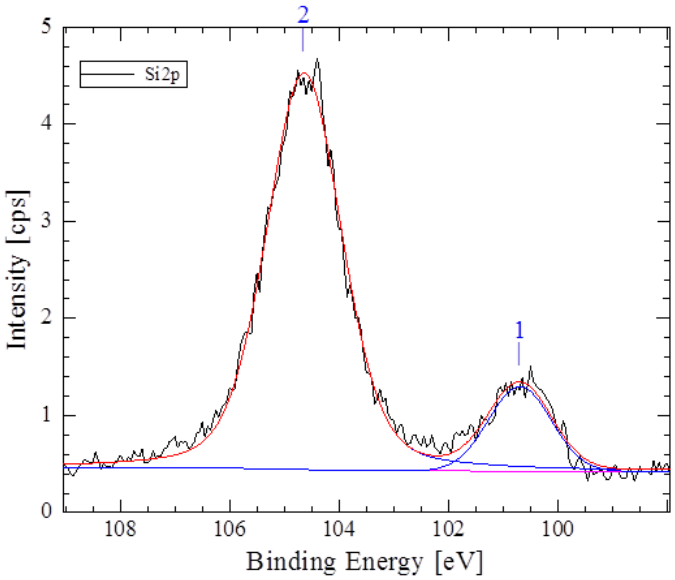

Figure 3.31: Example of fitted Si XPS spectra.

In order to provide a hydrophilicity composition profile along the p-Si pores, we decided to consider the ratio between the Bromo and the carboxylic group signal area as a figure of merit. Since this parameter links the amount of groups containing Bromo in respect to the carboxylic groups, we decided to call it "index of hydrophilicity".
In Figure 3.32 we report the depth profiling of the index of hydrofilicity with respect to the tilting angle.

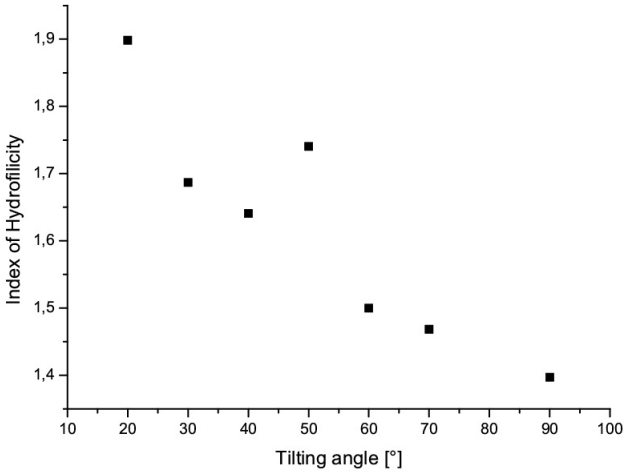

Figure 3.32: Hydrophilicity profile

The results show that the hydrophilicity increases approaching the surface, this suggest that we were able to properly differentially functionalize the inner hydrophobic and outer hydrophylic surface. This trend is in perfect agreement we what we expected both from our theoretical hypothesis and from the other characterizations already treated.

3.0.10 Raman spettroscopy

Raman measurements were performed to verify if we introduced an uniform functionalization layer all throughout the surface of the pores, in particular we wanted to check the ability of the liquid masking to protect the functionalization inside the pores.

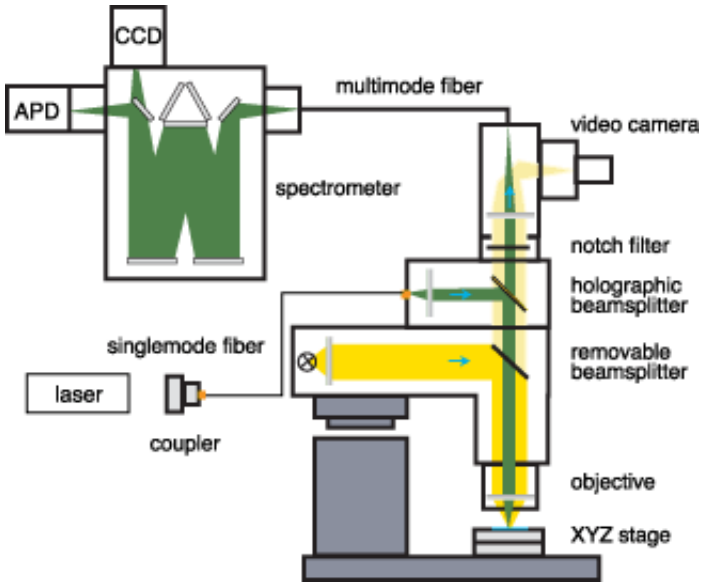

Figure 3.33: HORIBA Scientific LabRAM ARAMIS working sceme.

Data collection

The raman spectra were acquired on HORIBA Scientific LabRAM ARAMIS using a 633nm exciting light, with both emission and excitation slit at 1000nm and an attenuation of $\times 4$. We set the time of collection to 5 acquisition per second for 10 seconds and mediated over 5 spectra.

This kind of analysis was performed on the end result of a functionalization procedure on a non-luminescent porous silicon starting material, in particular we used 11-Bromo-1-undecene for the first hydrosilylation and then proceeded with a 1% Hf acid attack and a second hydrosilylation using acrylic acid.

For the analysis we cut the sample in half and mounted it on an appropriate support, making us able to perform a cross sectional examination.

Data analysis

In Figure 3.34 we report the Raman spectra of the samples at different sample depth.

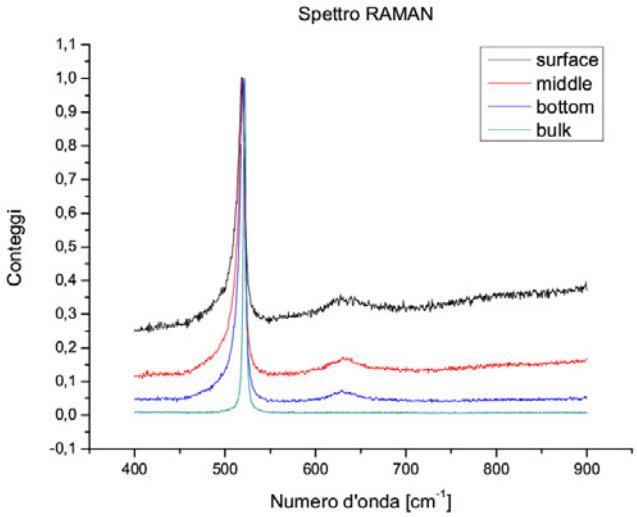

Figure 3.34: Raman spectra of non luminescent porous silicon layer.

The band of the Bromo is clearly visible at $\lambda = 647 cm^{-1}$ [33] in all three spectra corresponding to the porous portion of the sample.
We can then say that the porous walls are still functionalized after the acid attack and the new functionalization. [45][46] Unfortunately we cant say anything about a variation of the bromo amount correspondent to the different position of acquisition. The laser dot is indeed large enough to not let us distinguish properly the external surface from the entrance of the pores. This fact is coherent with what we find fitting the peaks,the areas of all three peaks are compatible within the errors.

Chapter 4

Conclusions

The aim of this thesis work was to obtain a bifunctional p-Si material presenting hydrophilic external surface and hydrophobic inner pore walls, strongly luminescent and highly stable, highly biodegradable and biocompatible. The p-Si microparticles were modified in order to be used as drug delivery system and at the same time as florescent probes allowing us to follow them during their journey.
This objective was reached with validation of the following types of characterization: Photoluminescence Spectroscopy, Fourier Transform Infrared Spectroscopy (FTIR), X-ray photoelectron spectroscopy (XPS), Contact angle and Raman Spectroscopy.

Porous silicon was produced in order to examine the validity of the liquid masking approach and if it can produce a selectively functionalized p-Si nanostructures with controllable hydrophobicity/hydrophilicity characteristics.
Two differently etched porous silicon kinds, and a three step surface modification procedure, were studied. Different porous silicon samples where exploited on the basis of their original optical and morphological properties to perform the different type of analysis required for our study. In particular we produce luminescent porous silicon microparticles (size the particle about $10\mu m$ with pore diameter about 30 nm) and non luminescent porous silicon layer (depth of the layer about $44\mu m$ with pore diameter about 30 nm).
They were used respectively for Photoluminescence Spectroscopy, Fourier Transform Infrared Spectroscopy (FTIR), Contact angle and Raman Spectroscopy, X-ray photoelectron spectroscopy (XPS) and Contact angle.

We found that:

- the pores are properly functionalized till the bottom(Raman analysis)

- a hydrophobicity profile is present inside the pore, i.e. the surface is strongly hydrophobic inside the pore and it becomes hydrophilic approaching the outer surface of the porous particle. This aspect its strongly emphasized by the XPS analysis which suggest the presence of a hydrophobicity profile along the p-Si pores.

- This hydrophobic profile is compatible with the carboxylic functionalization profile present inside the pore suggested by the FTIR analysis, i.e. the surface exhibits sparsely carboxylic chains inside the pore and it becomes covered in them approaching the outer surface of the porous particle.

- The resulting surface displayed contact angle raging from 45° to 72°, depending on the type of silicon used, in accord with a hydrophilic character of the outer surface.

- from the contact angle analysis we found that after the first hydrosilylation with heptene the surface was properly functionalized and that the acid attack truly removes the $Si - CH_2$ and $Si - CH_3$ in order to replace them with the Si-COOH after the second hydrosilylation. We also found that 1% Hf is enough to remove the grafted molecules from the external surface.

- Finally, we have proved that the final product of our procedure are microparticles which are still strongly luminescent and the PL decay is compatible with the time required by in vivo delivery (the PL is well detectable after 10 days). So their fate inside the cells can be monitored directly without the use of fluorescent labels.

Further experiments that needs to be done are:

- controlled drug release experiment using an hydrophobic test molecule.

- controlled release of small molecules paying particular attention to the rate of release compared to the degree of surface modification.

Moreover thanks to this thesis work I had the opportunity to meet Ali Ghafarinazari (Verona University) and to start a collaboration that led to the production of a conference paper: "Kinetics for Oxidation of Mesoporous Silicon" and to an article currently under review.

Appendix A

Choice of the Starting Materials

In this section we are going to present the results that led us to the choice of the starting materials. As described in "Naked porous silicon" we needed two different types of preparation: a luminescent and a non-luminescent one.

A.0.11 Non Luminescent porous silicon

As previously discussed in section "Naked porous silicon" this kind of material was needed in order to be able to perform some of the characterization analysis.
For this type of analysis we required: the sample to be pitch black, the thickness of the porous silicon layer to be some tenth of a micron and to have pore size around 10-30nm. In table A.1 are reported the results of our analysis divided on the bases of the starting material and on the electrochemical etching characteristics. The photolumunescence emission ability was checked by eye inspection irradiating the sample by an UV lamp while for the depth was used the XploRA ONE microscope.

[a]Boron, N-0.01-0.02 $\Omega \cdot cm$, $< 100 >$			
[b]I$[mA/cm^2]$	T[min]	solution	note
15	5	ETOH:HF(16%)	less than 5 μm
20	5	ETOH:HF(16%)	less than 5 μm
50	5	ETOH:HF(16%)	less than 5 μm
15	5	H_2O:HF(6%)	less than 5 μm
10	7	ETOH:HF(16%)	less than 5 μm
15	8	ETOH:HF(16%)	less than 5 μm
10	5	ETOH:HF(30%)	less than 5 μm
10	8	ETOH:HF(30%)	less than 5 μm
15	5	ETOH:HF(30%)	less than 5 μm
30	5	ETOH:HF(30%)	less than 5 μm
5	5	ETOH:HF(30%)	less than 5 μm
5	1	ETOH:HF(25%)	less than 5 μm

[a]Boron,N-0.01 $\Omega \cdot cm$, $< 100 >$			
10	5	ETOH:HF(16%)	near to elettropolishing
70	2	ETOH:HF(16%)	elettropolishing
70	2	ETOH:HF(10%)	elettropolishing
5	5	ETOH:HF(16%)	quite dark
5	8	ETOH:HF(16%)	less than 5 μm
5	20	ETOH:HF(30%)	pitch black
5	20	ETOH:HF(20%)	pitch black
5	30	ETOH:HF(20%)	pitch black
5	30	ETOH:HF(16%)	pitch black

Table A.1: Etching conditions of various crystalline silicon samples and some morphological (layer uniformity) and optical (light emission) of the obtained pSi sample. a) Crystalline silicon characteristics: doping, resistivity, crystalline planes, b) etching conditions: current applied, etching time, electrolytic solution.

The last four are the only ones exploitable for our project. We proceeded by checking the porous silicon layer depth. For each sample we collected 2 images with different magnifications (50x and 100x) using XploRA ONE, then we proceeded to select the clearer images and to analyze them using the program Imagej for image analysis. For each sample (example Fig.A.6) we measured the layer depth in 5 different points and then mediated. The results are reported in tableA.2.

[a]Boron,N-0.01-0.02 $\Omega \cdot cm$, $< 100 >$			
[b]I[mA/cm^2]	T[min]	solution	depth
5	20	ETOH:HF(30%)	8 ± 1
5	20	ETOH:HF(20%)	8 ± 1
5	30	ETOH:HF(20%)	9 ± 1
5	30	ETOH:HF(16%)	10 ± 1

Table A.2: Porous silicon layer depth.a) Crystalline silicon characteristics: doping, resistivity, crystalline planes, b) etching conditions: current applied, etching time, electrolytic solution.

Checking in the literature [20] we can found that the pore diameter corresponding to the last preparation (Boron,N-0.01-0.02 $\Omega \cdot cm$ $5mA/cm^2$, $T = 30min$ and $ETOH : HF(16\%)$)is estimated to be around 20nm.
For these reasons for our work we used the p-Si produced using the following conditions:

- material: Boron doped silicon, N-type, resistivity: 0.01-0.02 $\Omega \cdot cm$, orientation: $< 100 >$,

- etching conditions: intensity:$5mA/cm^2$, etching time: 30 min, solution: ETOH:HF(16%).

This non-luminescent porous silicon material was used for: contact angle, Raman and XPS analysis. In Figure A.1 is reported the optical image of freshly etched micro-pSi layer.

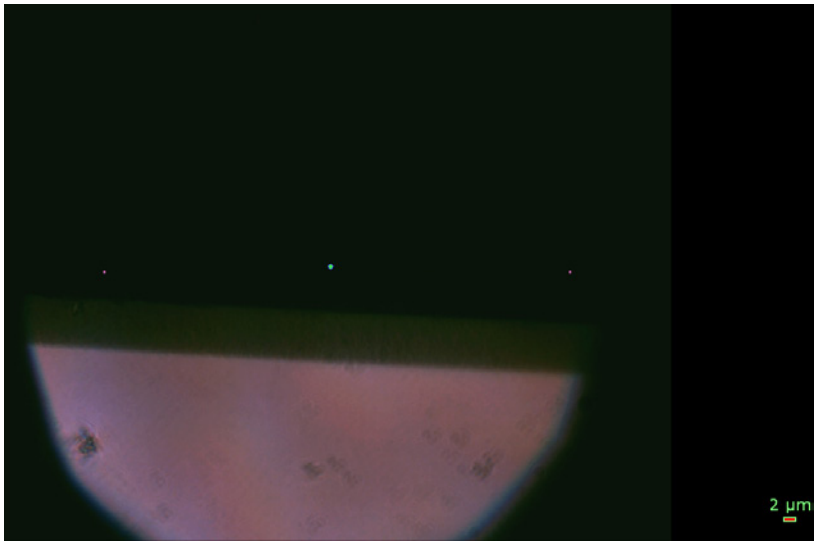

Figure A.1: Optical image (magnification 100x) of freshly etched micro-pSi layer.

To better characterize our material we produced a gravinometrical index of porosity using the approximated formula:

$$P(\%) = \frac{m_1 - m_2}{m_1 - m_3}$$

where m_1 is the weight of the wafer before the etching, m_2 is the weight of the wafer right after the etching and m_3 is the weight of the wafer after the removal of the porous layer.
The result is $P(\%) = (70 \pm 7)\%$.

A.0.12 Luminescent porous silicon

The aim of our work was to obtain silicon microparticle differentially functionalized and suitable as drug delivery system. This requires the particle to have dimensions small enough to be able to favorably interact with the biological environment and dimension and inner structure suitable to the biomolecule they are intended to interact with.
In our case this corresponded to particle's dimension of some tenth of a micron and pore diameter around 10-50nm. Also, since we wanted to be able to follow them during their journey, we wanted them to be luminescent: the most suitable PL is the red near infrared region of the EM spectrum.
Using the electrochemical etching procedure described in "Naked porous silicon" section we prepared a vast variety of samples changing every time one of the following parameters: current, time, etching solution and starting material.
These results are reported in table A.4 along with a first rough PL examination.
In bold character we have highlighted the most promising preparations.
This first analysis was followed by the characterization of the morphological structure and PL of the particles.

Boron, P-10 $\Omega \cdot cm$, $< 100 >$
The samples obtained from the first type of silicon(Boron,P-10 $\Omega \cdot cm$, $< 100 >$) were too small and after sonication we weren't able to separate them from the supernatant by centrifugation and for this reason For this reason we couldn't utilized this samples.

Boron, P-3-6 $\Omega \cdot cm$, $< 111 >$
The PL spectrum of 1mg of p-Si powder suspended in 2ml toluene was collected using Varian Cary Eclipse Fluorescence Spectrometer and is reported in Figure A.2.
From Figure A.2 we can see an intense PL peaked at $\lambda = 655 \pm 5nm$. The intensity decreases with time and shifts at shorter wavelength, but it stabilizes after 3 days at 603 nm.

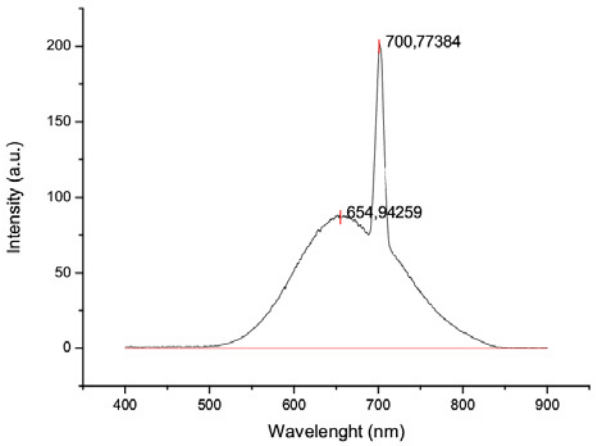

Figure A.2: PL of 1mg micro p-Si suspended in 2ml toluene.The photoluminescence was tested using a 350-300nm exciting light, with both emission and excitation slit at 10nm this allow us to reach a resolution of 5nm.

By optical microscopy we observed that the dimensions of the p-Si particles are in the range 1-15 μm as shown in Figure A.3.

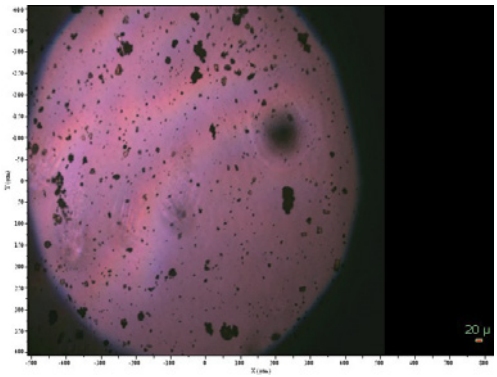

Figure A.3: Optical image (magnification 50x) of freshly etched micro-pSi particle.

This preparation seemed really promising although we found out that, after a functionalization with heptene and the treatment with HF, the silicon structure becomes very fragile and breaks during the next step of functionalization.

Boron, P-10-20 $\Omega \cdot cm$, $< 100 >$,70mA and 15 min
This is the material we end up using for our work.
As for the previous cases we checked the PL and the morphology.

Luminescence

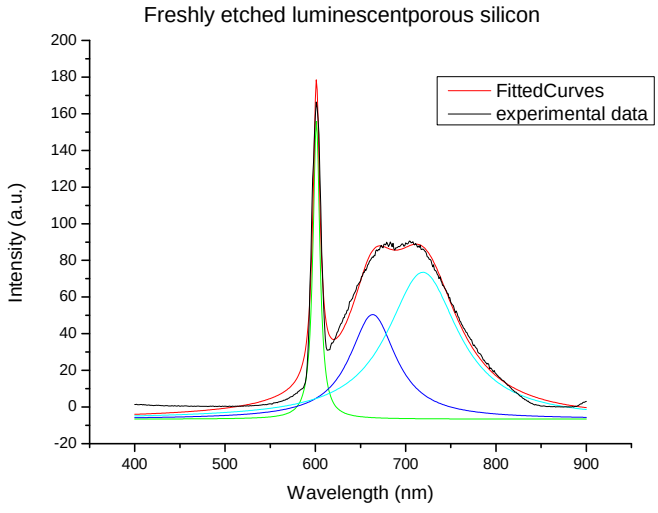

Figure A.4: Photoluminescence of 1mg micro-pSi after the second functionalization with acrylic acid suspended in 2ml toluene.Again in this case there is only one red band. In figure we reported in green the gaussian deconvolution curves, in red the fitting one and in black the data collected.

In Figure A.4 is clearly visible the presence of two distinct red band emission, properly described through the gaussian deconvolution. As we have previously seen the emission wavelength is strongly linked to the silicon morphology suggesting the presence inside the sample of two different family of silicon nanostructures.
The results of the gaussian deconvolution are the following:

- $\lambda = (719 \pm 5)nm$ and $I = (89 \pm 6)a.u.$
- $\lambda = (663 \pm 4)nm$ and $I = (84 \pm 5)a.u.$

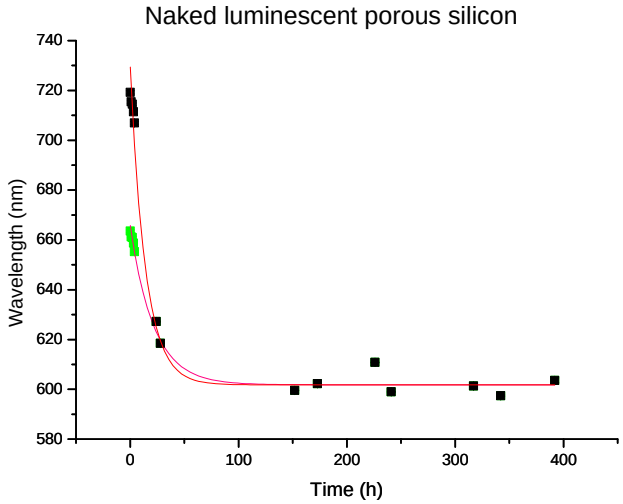

Figure A.5: Time dependance emission wavelength of 1mg of naked micro p-Si suspended in 2ml toluene. In black is reported the aging process of the band with the higher starting wavelength, the green points are the peak wavelength history of the band with the lower starting wavelength.The red and purple curves are the exponential fit relative to the two different families of emitting structures.

The luminescence emission within the limits of our analysis seems to reach a plateaux after approximately 30 hours as the wavelengths of the peak emission approaches $\lambda = (601 \pm 5)nm$ (Fig.A.5)

Morphology

Using the program Imagej for image analysis we chose the five best resolved particles from Figure A.6 and proceeded to measure their dimensions, the results were then mediated. The average particle size are $(13 \pm 3\mu m)$x$(4 \pm 2\mu m)$.

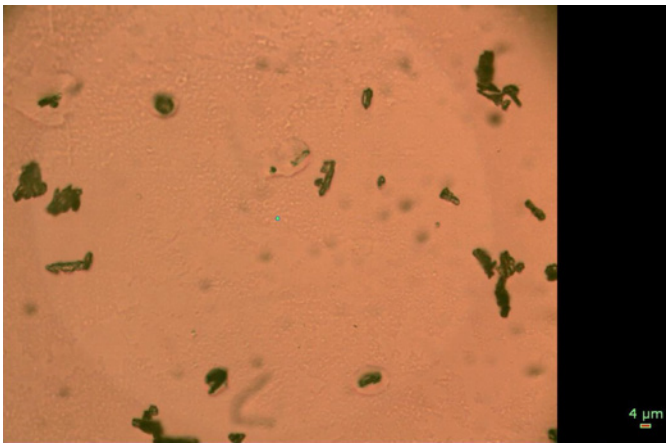

Figure A.6: Optical image (magnification 50x) of freshly etched micro-pSi particles.

The average silicon layer thickness is $(44 \pm 2\mu m)$ and gravinometrical index of porosity is $P(\%) = (77 \pm 3)\%$. Again the result was obtained through repeated measurements on the particle in Fig.A.6 using the program Imagej.

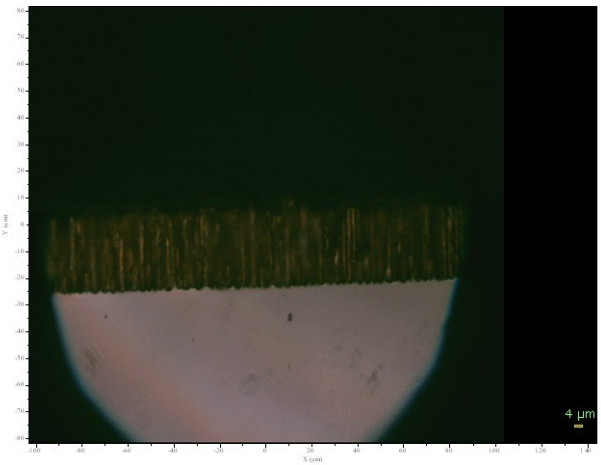

Figure A.7: Optical image (magnification 50x) of freshly etched micro-pSi layer.

The other five preparations relative to the same starting material were discharged for different reasons, for example we choose the preparation that granted us the best compromise between porous silicon layer depth and structural stability.

^{a}I$[A/cm^2]$	T[min]	Depth$[\mu m]$
70	3	18 ± 2
70	8	20 ± 2
70	15	44 ± 2
50	5	11 ± 1
60	15	9 ± 1

Table A.3: Porous silicon layer depth. a) etching conditions: current applied, etching time, electrolytic solution.

[b]I[mA/cm^2]	T[min]	solution	note
[a]Boron,P-10 $\Omega \cdot cm$, $< 100 >$			
70	5	ETOH:HF(16%)	not uniform, not luminescence
80	5	ETOH:HF(16%)	not uniform, not luminescence
85	5	ETOH:HF(16%)	not uniform, not luminescence
75	5	ETOH:HF(16%)	not uniform, not luminescence
65	5	ETOH:HF(16%)	not uniform, not luminescence
10	5	ETOH:HF(11%)	not uniform, light red luminescence
15	5	ETOH:HF(11%)	not uniform, light red luminescence
20	5	ETOH:HF(11%)	uniform, red luminescence only on the edge
25	5	ETOH:HF(11%)	uniform, red luminescence only on the edge
35	5	ETOH:HF(11%)	uniform, not homogeneously luminescence
40	5	ETOH:HF(11%)	not uniform, not homogeneously luminescence
28	**5**	**ETOH:HF(11%)**	**uniform, high red luminescence**
28	**5**	**ETOH:HF(11%)**	**uniform, high red luminescence**
27	5	ETOH:HF(11%)	uniform, not homogeneously red luminescence
28	17	ETOH:HF(11%)	not uniform, not luminescence
[a]Boron,P-3-6 $\Omega \cdot cm$,$< 100 >$			
27	5	ETOH:HF(16%)	not uniform, not luminescence
70	5	ETOH:HF(16%)	not uniform, not luminescence
28	5	ETOH:HF(16%)	not uniform, not luminescence
10	5	ETOH:HF(16%)	not uniform, not luminescence
[a]Boron,P- 3-6 $\Omega \cdot cm< 111 >$			
75	5	ETOH:HF(16%)	uniform, red luminescence on the edge
65	5	ETOH:HF(16%)	light orange luminescence
50	5	ETOH:HF(16%)	high reddidh luminescence
50	15	ETOH:HF(16%)	uniform, unevenly luminescence
50	15	ETOH:HF(11%)	uniform, not luminescence
45	5	ETOH:HF(16%)	orange luminescence
20	5	ETOH:HF(16%)	light orange luminescence
75	5	ETOH:HF(16%)	light orange luminescence
10	**5**	**ETOH:HF(16%)**	**extremely high red luminescence**
10	15	ETOH:HF(16%)	light orange luminescence
10	5	HF:H_2O:DMSO(4M)	not luminescence
10	10	HF:H_2O:DMSO(4M)	not luminescence
15	10	HF:H_2O:DMSO(4M)	not luminescence
10	5	HF:H_2O:DMSO(4M)	not luminescence
8	5	HF:H_2O:DMSO(4M)	not luminescence
10	10	HF:H_2O:DMSO(4M)	not luminescence
10	10	HF:H_2O:DMSO(8M)	not luminescence
8	10	HF:H_2O:DMSO(8M)	not luminescence
10	10	HF:H_2O:DMSO(8M)	not luminescence
8	10	HF:H_2O:DMSO(8M)	not luminescence

[a]Boron, P-10-20 $\Omega \cdot cm$, $< 100 >$			
80	5	ETOH:HF(16%)	not uniform
70	5	ETOH:HF(16%)	not uniform, uneven red luminescence
60	**5**	**ETOH:HF(16%)**	**high red luminescence**
70	**5**	**ETOH:HF(16%)**	**high red luminescence**
70	**3**	**ETOH:HF(16%)**	**high red luminescence**
70	**8**	**ETOH:HF(16%)**	**high red luminescence**
60	**15**	**ETOH:HF(16%)**	**high red luminescence**
50	**15**	**ETOH:HF(16%)**	**light red luminescence**

Table A.4: Results of our trial tests. a) Crystalline silicon characteristics: doping, resistivity, crystalline planes, b) etching conditions: current applied, etching time, electrolytic solution.

Bibliography

[1] O. Bisi, S.Ossicini, L.Pavesi, *Porous silicon: a quantum sponge structure for silicon based optoelectronics*, Surface Scuence Reports 38(2000)1-126.

[2] L.T.Canham, silicon structure fabrication through nanoetching techniques, Adv.Mater.(1995), 7, 10331037.

[3] V.Lehemann, *Elechtrochemistry of silicon: instrumentations, science, materials and applications.*, Wiley, (2002), 1, 286-288.

[4] E.A. Fitzgerald and L.C. Kimerling, *Silicon-Based Microphotonics and Integrated Optoelectronics*, MRS BULLETIN/APRIL 1998.

[5] A.Abbott, *Betting on tommorow's chips*, Nature (2002), 415 (6868), 112-114.

[6] M.E.Akerman, W.C.W.Chan, P.Laakkonen, S.N.Bhatia, E.Ruoslahti, *Nanocrystal targeting in vivo*, PNAS (2002), 99(20), 12617-12621.

[7] A.Uhlir, *Electrolytic Shaping of Germanium and Silicon* Bell Syst.Technol.J. (1956), 35, 333.

[8] S.Ossicini, L.Pavesi, F.Priolo, *Light emitting silicon for microphotonics*, Springer Tracts in modern Physics, vol.194(2003),75-121.

[9] L.Gu et al. *Magnetic luminescent porous silicon microparticles for localized delivery of molecular drug payloads*, Small, 2010, 6(22), 2546-2552.

[10] L:Pavesi, M.Ceschini, G.Mariotto, E.Zanghellini, O.Bisi, M.Anderle, L.Calliari, M.Fedrizzi and L.Fedrizzi, *Spectroscopic investigation of electroluminescent porous silicon*, Journal of Applied Physics 75, 1118(1994); doi: 10.1063/1.356495.

[11] Chia-Chen Wu and Michael J. Sailor, *Selective functionalization of the internal and the external Surface of Mesoporous Silicon y Liquid Masking*, American Chemical Society (2013),7(4), 3158-3167

[12] D.Liu, E.Mäkilä, H.Zhang, B.Herranz, M.Kaasalainen, P.Kinnari, J.Salonen, J.Horvonen and H.A.Santos, *Nanostructured Porous Silicon-Solid Lipid Nanocomposite: Toward Enhanced Cytocompatibility and Stability, Reduced Cellular Association and Prolongrd Drug Release*, Adv. Funct. Mater. (2013), 23, 1893-1902.

[13] J.Shen, R.Xu, J.Mai, H.C.Kim, X.Guo, G.Qin, Y.Yang, J.Wolfram, C.Mu, X.Xia, J.Gu, X.Liu, Z.W.Mao, M.Ferrari and H.Shen *High capacity nanoporous silicon carrier for systemic delivery of gene silencing therapeutics*, ACS Nano 2013, 7, 9867-9880.

[14] R.E.Serdaa, B.Godina, E.Blancoa, C.Chiappinib, M.Ferraria *Multi-stage delivery nano-particle systems for therapeutic applications*, Biochimica Biophysica Acta 2011, 1810, 317-329.

[15] M.A.Töllia, M.P.A.Ferreirab, S.M.Kinnunenc, J.Rysäa, E.M.Mäkiläb, Z.Szabóa, R.E.Serpia, P.J.Ohukainena, M.J.Välimäkia, A.M.R.Correiab, J.J.Salonene, J.T.Hirvonenb, H.J.Ruskoahoa, H.A.Santos, In vivo biocompatibility of porous silicon biomaterials for drug delivery to the heart, Biomaterials 2014, 35, 8394-8405.

[16] E.Secret, K.Smith, V.Dubljevic, E.Moore, P.Macardle, B.Delalat, M.L.Rogers, T.G.Johns, J.O.Durand, F.Cunin and N.H.Voelcker *Antibody-Functionalized Porous Silicon Nanoparticles for Vectorization of Hydrophobic Drugs* Advanced Healthcare materials 2013, 2, 718-727.

[17] H. Föll, *Properties of silicon-electrolyte junctions and their application to silicon characterization*, Applied Physics A (1991), Volume 53, Issue 1, pp 8-19

[18] R. L. Smith and S. D. Collins, *Porous silicon formation mechanisms* , J. Appl. Phys. 71, R1 (1992).

[19] V.Lehmann and U.Gösele, *Porous silicon formation: A quantum wire effect* Appl.Phys.Lett.(1991),58,856.

[20] V. Lehmann and H. Föll, *Formation Mechanism and Properties of Electrochemically Etched Trenches in n-Type Silicon*, Journal of Electrochemical Society,(1990),vol.137,issue2,653-659.

[21] M.I.J.Beale, J.D.Benjamin, M.J.Uren, N.J.Chew, A.G.Cullis, *An experimental and theoretical study of the formation and microstructure od porous silicon*, J.of Crystal Growth (1985),73, 622-636.

[22] X.J.Zhang, *Mechanism of pore formation on n Silicon*, J. Electrochem. Soc.(1991), 138(123), 3750.

[23] H.Foll, J.Cartensen, M.Christophersen, G.Hasse, *A new view on silicon electrochemistry*, Phys.Stat.Sol,(a)(2000), 182, 7-16.

[24] M.Nahidi and K.W.Kolasinski, *Effects of Stain Etchant Composition on the Photoluminescence and Morphology of Porous Silicon*, Journal of the Electrochemical Society, 153 (1) C19-C26, (2006).

[25] V.Lehmann, R.Stengl and A.Luigart, *On the morphology and the electrochemical formation mechanism of mesoporous silicon*, Mateials Science and Engineering B69-70 (2000) 11-22.

[26] C.Delurue, G.Allan, M.Lannoo, *Theoretical aspects of the luminescence of porous silicon*, Phys.Rew.B (1993), 48, 11024-11036.

[27] F.Koch, V.Petrova-Koch, T,Muschik, *The luminescence of porous Si: the case for the surface state mechanism*, J.Of Luminescence (1993), 57, 271-281.

[28] J.E.Bateman, R.D.Eagling, D.R.Worral, B.R.Horroks, A.Houlton, *Alkylation of Porous Silicon byDirect Reaction with Alkenes and Alkynes*, Angew. Chem. Int. Ed. (1998), 37(19), 2683-2685.

[29] X.Li, Y.He, M.T.Swihart, *Water-soluble Poly(acrylic acid) Grafted Luminescent Silicon Nanoparticles and Their Use as Fluorescent Biological Stianing Labels*, Nano Letters (2004), 4(8), 1463-1467.

[30] Leduox, G., O.Guillois, D. Porterat, C.Reynaud, F.Huisken, B.Kohn and V.Paillard, *Photoluminescence properties of silicon nanocrystals as a function of their size*, Phys.Rev.B(2000),62(23),15942-15951.

[31] Leduox, G., J.Gong and F.Huisken, *Effects of passivation and aging on the photoluminescence of silicon nanocrystals*, Appl.Phys.lett.(2001),79(24),4028-4030.

[32] J.M.Buriak, *Silicon-carbon bonds on porous silicon surfaces*, Advanced materials(1999),11(3).265-267.

[33] Forrest F. Cleveland and M. J. Murray, *Raman Spectrum of 1-Bromo-Dodecane*, The Journal of Chemical Physics 8, 867 (1940).

[34] E.J.Lee,T.W.Bitner,J.S.Ha,M.J.Shane, M.J. Sailor, *Light-induced reaction of porous and single-crystals Si surfaces with carboxylic acids*, J.Am.Chem.Soc(1996),1118,5375-5382.

[35] E.Froner, R.Adamo, Z.Gaburro, B.Margesin, L.Pavesi, A.Rigo, M.Scarpa, *Luminescence of porous silicon derived nanocrystals dispersed in water: dependence on initial porous silicon oxidation*, Journal of Nanoparticle Research,December 2006, Volume 8, Issue 6, pp 1071-1074

[36] Ledoux G.,Guillois O., Porterat D., Reynaud C., Huisken F., Kohn B. & Paillard V., *Photoluminescence properties of silicon nanocrystals as a function of their size*, Phys.Rev.B (2000), 62(23), 15942-15951.

[37] J.L. Heinrich, C.L. Curtis, G.M. Credo, M.J. Sailor and Kavanagh, *Luminescent colloidal silicon suspensions from porous silicon*, Science,(1992),255,66-68.

[38] A. Grill, *Porous pSICOH Ultralow-k Dielectrics for Chip Interconnects Prepared by PECVD*, Annual Review of Materials Research, (2009), Vol. 39: 49-69

[39] P.J.Launer *Infrared analysis of organosilicon compounds: spectra-structure correlations*, Laboratory for materials, Inc., Burnt Hills, New York 12027.

[40] P.J.Launer, *Infrared analysis of organosilicon compounds:spectra-structure correlations* , Laboratory for Materials, Inc., Burnt Hills, New York 12027.

[41] C.S. Fadley, *Angle resolved X-ray photoelectron spectroscopy*, progress In Surface, vol.16pp.275-388,1984.

[42] S. Hajati and S.Tougaard, *XPS for non-destructive depth profiling and 3D imaging of surface nanostructures*, Anal. Bioanal. Chem (2010), 396, 2741-2755.

[43] A.V.Merzlikin, N.N.Tolkachev, T.Strunskus, G.Witte, T.Glogowski, C.Woll, W.Grünert, *Resolving the depth coordinate in photoelectron spectroscopy-Comparison of excitation energy variation vs. angular-resolved XPS for the analysis of a self-assembled monolayer model system*, Surface Science 602 (2008) 755-767.

[44] D.A. Shirley, *High-resolution X-ray photoemission spectrum of the valence bands of gold*, Phys.Rev 55,4709(1972).

[45] S.Trusso, C.Vasi, M.Allegrini, F.Fuso and G. Pennelli, *Micro-Raman study of free-standing porous silicon samples*, Journal of vacuum Science Technology B 17, 468 (1999); doi: 10.1116-1590578.

[46] M.N Islam, A.Pradhan and S.Kumar, *Effects of crystallite size distribution on the Raman-scattering profiles of silicon nanostructures* Journal of Applied Physics 98, 024309(2005); doi: 10.1063/1.1980537.

[47] John Coates, *Interpretation of Infrared Spectra, A Practical Approach*, Encyclopedia of Analytical Chemistry,(2000) R.A. Meyers (Ed.) 10815 10837,John Wiley Sons Ltd, Chichester.

[48] Alfred Grill, *Porous pSICOH Ultralow-k Dielectrics for Chip Interconnects Prepared by PECVD* , Annual Review of Materials Research, Vol. 39: 49-69.

[49] M.A.Tishler, R.T.Collins, J.H.Stathis, J.C.Tsang, *Luminescence degradation in porous silicon* , Appl.Phys.Lett.(1992),60,639.

[50] H.Ono,H.Gomyou,H.Morisaki, S.Nozaki, Y. Show, MShimasaki, M.Shimasaki, M.Iwase, T.Izumi, *Effects of Anodization Temperature on Photoluminescence from Porous Silicon*, J. Electrochem.Soc.(1993),140,L180.

[51] A. G. Cullis, L. T. Canham, P. D. J. Calcott, *The structural and luminescence properties of porous silicon*, J. Appl. Phys. 1997, 82, 909-965.

[52] James E. Bateman, Robert D. Eagling, David R. Worrall, Benjamin R. Horrocks,* and Andrew Houlton *Alkylation of Porous Silicon by Direct Reaction with Alkenes and Alkynes*, Angew. Chem. Int. Ed.1998,37, No. 19.

[53] Michael P. Stewart and Jillian M. Buriak *Photopatterned Hydrosilylation on Porous Silicon*, Angew. Chem. Int. Ed. 1998, 37, No. 23.

[54] X.Cheng, S.B.Lowe,P.J.Reece and J.J.Gooding, *Colloidal silicon quantum dots: from preparation to the modification of self- assembled monolayers (SAMs) for bio-applications*, Chem.Soc.Rev. 2014, 43, 2680-2700.

[55] C.Xu, G.Guo, L.Gui, Y.Tang, B.R.Zhang and G.G.Qin, *Optical properties and luminescence mechanism of oxidized free-standing porous silicon film*, Journal of Applied Physics 86, 2066(1999); doi:10.1063/1.371010.

[56] N.Brunetto and G.Amato, *A new line shape analysis of Raman emission in porous silicon*, Thin solid Film 297 (1997), 122-124.

[57] I.M.D.Höhlein, J.Kehrle, T.K.Purkait, J.G.C.Veinot and B.Rieger, *Photoluminescent silicon nanocrystals with chlorosilane surface-synthesis and reactivity*, Nanoscale, (2015), 7, 914-918.

[58] L.M.Wheeler, N.R.Neale, T.Chem and U.R.Kortshagen, *Hypervalent surface interaction for colloidal stability and doping of silicon nanocrystals*, Nature communications (2013) doi:10.1038.

[59] F. Priolo, T. Gregorkiewicz M.Galli and T.F.Krauss, *Silicon nanostructure for photonics and photovoltaics*, Nature Nanotechnology, (2014), vol.9

[60] E.A.Angelopoulos, S.Ferwana, MZimmermann, E.Penteker and J.N.Burghartz, *Poruos Silicon for Micro- and Optpelectronic Applications. Fabrication Technology and Post-Processing Step*,

[61] F.A.Harraz, K.Kamada, K.Kobayashi, T.Sakka and Y.H.Ogata, *Random Macropore Formation in p-Type Silicon in HF-Containing Organic Solutions*, Journal of the elctrochemical society, 152 (4), C213-C220 (2005).

[62] V.Lehmann and S.Rönnebeck, *The Physics of macropore formation in Low-Doped p-type Silicon*, Journal of the Electrochemical Society, 146 (8), 2968-2975 (1999).

[63] B.Gelloz, A.Loni, L.Canham and N.Koshida, *Luminescence of mesoporous silicon powders treated by high-pressure water vapor annealing*, Nanoscale Research Letters (2012) vol.7, 382.

[64] B.Gelloz, T.Shibata and N.Koshida, *Stable elestroluminescence of nanocrystalline silicon device activated by high pressure wapor annealing*, Applied Physic Letters 89 191103(2006).

[65] J.P.Wilcoxon and G.A.Samara, *Tailorable, visible light emission from silicon nanocrystals*, Applied Physics Letters vol.74 n.21.

[66] S.Chattopadhyay and P.W.Bohn, *Surfactant-Induced Modulation of Light Emission in Porous Silicon Produced by Metal-Assisted Electroless Etching*, Anal.Chem(2006), 78, 6058-6064.

[67] V.Lehmann, *Electrochemistry of silicon: instrumentation, science, materials and applications*, Science, Material ans applications(2002) 1, pp286.